Pricing Extreme Mortality Risk amid the COVID-19 Pandemic

Han Li[a], Haibo Liu[b,c], Qihe Tang[b], and Zhongyi Yuan[d]*

[a]Department of Actuarial Studies and Business Analytics, Macquarie University

[b]School of Risk and Actuarial Studies, UNSW Sydney

[c]Department of Statistics and Department of Mathematics, Purdue University

[d]Smeal College of Business, The Pennsylvania State University

August 3, 2021

Abstract

In pricing extreme mortality risk, it is commonly assumed that the interest rate and mortality rate are independent. However, the recent COVID-19 outbreak calls this assumption into question. We propose a bivariate affine jump-diffusion structure to jointly model the interest rate and excess mortality, allowing for both correlated diffusions and joint jumps. Utilizing the latest US mortality and interest rate data, we find a strong negative correlation between the jump sizes of interest rate and excess mortality, and a much higher jump intensity when the pandemic data is included. Moreover, we construct a risk-neutral pricing measure that accounts for both a diffusion risk premium and a jump risk premium. We then solve for the market prices of risk based on mortality bond prices. Our results show that the pandemic experience can drastically change investors' risk perception and will likely reshape the post-pandemic mortality risk market.

JEL classification: C32; C58; G13

Keywords: risk-neutral pricing; mortality-linked security; affine jump-diffusion model; implied market price of risk

*Corresponding author. Email address: zhongyi-yuan@psu.edu

1 Introduction

Mortality is a primary source of risk to life insurers. Shocks that lead to large-scale losses of life, commonly referred to as extreme mortality risk, can put life insurers' profitability and solvency under pressure. Nonetheless, it is perhaps not until the recent outbreak of the COVID-19 pandemic that the impacts of extreme mortality beyond the insurance industry and its capacity to change the landscape of the world economy are recognized. There is an urgent need to achieve a quantitative understanding of the impacts of the pandemic. In this paper, we tackle this issue from pricing of extreme mortality risk amid the COVID-19 pandemic.

Traditionally, insurance companies mitigate and manage extreme mortality risk by means of reinsurance. In recent decades, insurers have also used insurance-linked securities (ILS) for additional protection against solvency-threatening losses. As an innovative solution to mitigate and transfer insurance risk, ILS have formed a sizable market and have shown a very strong growth, with a current outstanding capital of around US$50 billion.[1] This great success can partly be attributed to a belief that catastrophe risk is uncorrelated with the other risks in a financial market and as such ILS bring diversification benefits. Their high returns also appeal to investors. Some recent reviews and studies of ILS can be found in Cummins (2008), Barrieu and Albertini (2009), Braun et al. (2019), Tang and Yuan (2019), and Liu et al. (2021), among others.

Along with the rapid development of the ILS market, various mortality-linked securities (MLS), and in particular mortality catastrophe (CAT) bonds, have proven to be an early success. In December 2003, Swiss Re issued the first mortality CAT bond of size US$400m via Vita Capital. During the risk period of the bond, if the underlying mortality index exceeds a certain threshold, the bond is triggered and the principal will be reduced or wiped out to compensate for insurance losses. Since then, numerous MLS have been issued, examples including Swiss Re Vita Capital II of size US$362m, Swiss Re Vita Capital III of size US$705m, Atlas IX Capital of size US$180m, and AXA Benu Capital of size EUR285m. See Lin and Cox (2008), Deng et al. (2012), Bauer and Kramer (2016), and Li and Tang (2019) for related discussions and see Blake and Cairns (2021) for a comprehensive review.

Pricing MLS requires accurate modeling of extreme mortality risk, as well as its interaction with other risks in the market. In the literature, a long-standing assumption in modeling, managing, and especially pricing mortality risk is the independence between the interest rate and mortality rate; see, e.g., Biffis (2005), Lin and Cox (2008), Bayraktar et al. (2009), Chen et al. (2015), and Menoncin and Regis (2020). However, as we have witnessed, the COVID-19 outbreak has triggered concurrent jumps, upward in mortality via a health shock and downward in interest rate via a financial shock, which calls the aforementioned independence assumption into question.

[1] For more detail, see `https://www.artemis.bm/dashboard/`.

In fact, the pandemic has already spawned a viewpoint among practitioners that extreme mortality and the performance of financial markets can be highly correlated.[2] We note that this correlation could be strong enough to distort the financial market and challenge some traditional views on market behavior and have profound implications for the future mortality risk market. In particular, if the low-correlation sentiment shifts, the demand in MLS may decline. This motivates us to examine the dependence between interest rate and mortality rate and address the issue in pricing MLS. As MLS are usually linked to an underlying mortality index in extreme mortality scenarios, we choose to model excess mortality rather than mortality rate itself.[3]

In this paper, we propose a bivariate affine jump-diffusion (AJD) structure to jointly model the interest rate and excess mortality so that we have an integrated setting to account for the frequency of joint jumps and the correlations between the two jump components and between the diffusions. It has been a common practice in asset pricing to incorporate infrequent but substantial jumps into the modeling framework. For example, Bates (1996) develops an exchange rate model for pricing American options on combined stochastic volatility jump-diffusion processes. Duffie et al. (2000) introduce the AJD structure for dynamic asset pricing models and provide a comprehensive analytical treatment to show its tractability in pricing financial securities. Since then AJD models have been widely used in finance, with early works including Kou (2002), Pan (2002), Eraker (2004), and Duffie (2005). In line with this trend, many studies on pricing life insurance products and mortality/longevity linked securities employ (affine) jump-diffusion models; see, e.g., Biffis (2005), Deng et al. (2012), and Lin et al. (2013).

The calibration of the proposed continuous-time AJD model requires mortality data of a higher frequency than annual, which has previously been difficult to acquire. Our empirical studies are possible thanks to the recent decision by the US Centers for Disease Control and Prevention (CDC) to collect and compile provisional death counts on a weekly basis, in response to COVID-19. Estimates of weekly excess deaths since January 2017 have also been published by CDC to provide information on the burden of mortality imposed by the pandemic. We are amongst the first to utilize this weekly mortality data to calibrate such a sophisticated model.

Utilizing the most up-to-date US mortality and interest rate data from 2017 to 2020, we conduct empirical studies to investigate the dynamics of interest rate and excess mortality processes. We calibrate the bivariate AJD model using the Markov Chain Monte Carlo (MCMC) method, based on an approximation of the transition density function proposed

[2]See, e.g., `https://www.cnbc.com/2020/03/18/coronavirus-world-bank-pandemic-bond-investors-face-big-losses.html` and `https://www.insurancejournal.com/news/international/2020/12/10/593490.htm`.

[3]Throughout this research, in a given time period, excess mortality is defined as the difference between the observed number of deaths and expected number of deaths, divided by the corresponding population exposure.

by Pienaar and Varughese (2016). Utilizing the full dataset which includes the pandemic data, we detect a significant number of joint jumps and find a strong negative correlation between the two jump components, while the two diffusions seem close to independent. When we only consider the pre-pandemic data, namely, data from 2017 to 2019, we detect much fewer joint jumps, but the estimated correlation coefficients for both jump and diffusion components almost remain unchanged.

We follow arbitrage pricing theory to develop a risk-neutral pricing measure that accounts for both diffusion risk and jump risk premia.[4] The diffusion risk premium is realized via a drift adjustment of the bivariate Brownian motion underlying the dynamics. Note that the jump risk is captured by multiple compound Poisson processes. To realize the jump risk premium, we follow Chapter 9 of Cont and Tankov (2004), and let each jump process remain a compound Poisson process under the pricing measure but with both the intensity and jump-size distribution adjusted, so that the jump risk premium applies to both the intensity and the size.

To gain better insights into the mortality risk market, we find the risk premia demanded by the MLS investors. To this end, we design a hypothetical mortality CAT bond that closely resembles the 2013 Atlas IX Capital Ltd. bond (hereafter, the Atlas bond). By assuming that the hypothetical bond would have been traded at the same prices as the Atlas bond if issued under the then market conditions, we solve for the market prices of risk (MPRs) based on the calibrated AJD model and by utilizing the price data of the Atlas bond. To understand the impact of the COVID-19 pandemic experience, we derive the investors' MPRs again, but instead assume a misalignment between the risk modeling agent's model and the actual model governing the risk processes—the former calibrated with pre-pandemic data only and the latter calibrated also with the pandemic data. We observe that the investors are earning much lower MPRs than in the previous case. In fact, the investors end up paying premia in this case due to overlooking the extreme mortality risk. Our analysis demonstrates the importance for market participants to use models that have properly accounted for the pandemic risk.

In addition, based on the estimated prices of the hypothetical bond, we conduct sensitivity analyses against the MPR parameters. As expected, an increase in any of the risk premia, ceteris paribus, will reduce the bond price. We find that the price is much more sensitive to changes in the jump risk premium than to the diffusion risk premium, which reaffirms the importance of incorporating the jump risk in our model.

[4]Tang and Yuan (2019) give a short review of various approaches to pricing ILS. In particular, the actuarial pricing approach takes the expectation under the physical measure of the sum of the discounted payoffs to get the expected present value and then applies a usually exogenous safety loading coefficient to produce the actuarial price of the ILS. This approach was prevailing in early times; see Galeotti et al. (2013) and references therein. However, in view of the rapid growth of the ILS market, it is important to estimate and incorporate the market price of (extreme) mortality risk to more accurately reflect investors' risk appetite.

The contribution of our research is twofold. First, we employ a bivariate AJD structure to jointly model the interest rate and excess mortality and calibrate the model by utilizing a newly compiled US mortality dataset that includes observations during the pandemic. We find that the joint jumps of the interest rate and excess mortality occur at a high frequency and lead to a strong negative instantaneous correlation between them. If the pandemic experience is excluded from the data, we observe less frequent joint jumps and a weakened instantaneous correlation. Second, building on the calibrated AJD model, we develop a risk-neutral pricing measure that accounts for both a diffusion risk premium and a jump risk premium. We then solve for the MPRs using second-market indicative mortality bond prices. Our results shed light on the mortality risk market in the post-pandemic era: the pandemic experience can shake the long-standing belief of independence between mortality risk and financial risk, and is likely to reshape the market.

The rest of the paper is organized as follows: Section 2 depicts the bivariate AJD model; Section 3 discusses the modeling and pricing frameworks of MLS; Section 4 illustrates our empirical results; Section 5 computes the implied MPRs under the AJD model calibrated for various scenarios, investigates the implications for the post-pandemic mortality risk market, and conducts sensitivity tests against the MPRs; Section 6 concludes the paper; the Appendix collects long proofs, derivations, and descriptions required for establishing our theory and sampling algorithm.

1.1 Connection to the World Bank pandemic bonds

It is interesting to notice that the insurance industry's innovation in extreme risk mitigation has recently been applied to disaster relief and post-event recovery by governments and international organizations. We end this section with a connection of our research to the World Bank's pandemic bonds. In 2017, drawing on lessons from the Ebola outbreak, the World Bank launched first-of-their-kind pandemic bonds to support a US$500 million pandemic emergency financing facility (PEF), with the intention to help the world's poorest countries to fight against cross-border, large-scale pandemic outbreaks. At issuance, the bonds were oversubscribed by 200%, indicating a strong demand from investors and great potential for health organizations to transfer pandemic risk to the capital market. The bonds matured in July 2020 and were triggered by the COVID-19 outbreak. However, the PEF has received a significant amount of criticism, mostly on its delayed payouts during the pandemic. Despite the World Bank's decision to scrap plans for a second issue of the pandemic bond, similar types of financial instruments will likely be developed in the future.

While mortality CAT bonds and pandemic bonds are essentially different financial instruments, we point out that our research on MLS sheds light on future pandemic bond pricing and design. First, the two types of bonds share similarities in triggering mechanisms, potential diversification benefits, and high coupon rates. Second, our results show that the COVID-19 experience can make a huge difference in the prices of mortality CAT

bonds. The World Bank's Class A pandemic bonds offered a 6.5% coupon rate, and the Class B pandemic bonds offered a 11.1% coupon rate, both notably higher than securities traded in the financial market. However, the investors' perception and appetite for future pandemic bonds are likely to change after this once-in-a-century pandemic and therefore future pandemic bond issuance should take into account the new information gathered during the COVID-19 pandemic. Third, taking a closer look at their respective stages of development, we anticipate further growth of the pandemic bond market. Issuers of future pandemic bonds may learn from the successful experience of mortality CAT bonds.

2 The affine jump-diffusion model

Throughout the paper, we use $\left(\Omega, \mathcal{F}, \{\mathcal{F}_t\}_{0\le t\le T}, P\right)$ to denote a filtered probability space that accommodates all sources of randomness, where $0 < T < \infty$ denotes the time horizon. Let $\{r_t\}_{0\le t\le T}$ be the interest rate process and $\{\mu_t\}_{0\le t\le T}$ be a mortality-linked reference process. The latter, unless otherwise stated, is specified as an excess mortality process to quantify extreme mortality risk. Denote by $\{\mathcal{F}_t^1\}_{0\le t\le T}$ and $\{\mathcal{F}_t^2\}_{0\le t\le T}$ the augmented natural filtrations generated by $\{r_t\}_{0\le t\le T}$ and $\{\mu_t\}_{0\le t\le T}$, respectively, and assume without loss of generality that $\mathcal{F}_t = \mathcal{F}_t^1 \vee \mathcal{F}_t^2$ for $0 \le t \le T$.

We will introduce a pricing measure Q. Then $E_t^Q[\cdot]$ represents the conditional expectation under Q given the information up to time t; that is, $E_t^Q[\cdot] = E^Q[\cdot|\,\mathcal{F}_t]$. Nevertheless, when an operation is under the physical probability measure P, we usually omit the superscript P for simplicity. Thus, Cov, Var, and $Corr$ denote the covariance, variance, and correlation under P, respectively.

2.1 Dynamics under P

Assume that the bivariate process $\{\mathbf{Y}_t = (r_t, \mu_t)^\intercal\}_{0\le t\le T}$ follows an affine jump-diffusion (AJD) process. Precisely, for $0 \le t \le T$,

$$d\mathbf{Y}_t = \mathbf{K}_t(\boldsymbol{\theta}_t - \mathbf{Y}_t)dt + \boldsymbol{\Sigma}_t\sqrt{\mathbf{S}_t}d\mathbf{W}_t + \sum_{i=1}^{m} d\mathbf{J}_{i,t}, \tag{2.1}$$

where

- the elements of $\mathbf{K}_t, \boldsymbol{\Sigma}_t \in \mathbb{R}^{2\times 2}$, and $\boldsymbol{\theta}_t \in \mathbb{R}^2$ are all deterministic functions of t;
- $\mathbf{W}_t = (W_{1,t}, W_{2,t})^\intercal$ for $0 \le t \le T$ is a standard bivariate Brownian motion;
- $\mathbf{S}_t$ is a diagonal matrix with the ith diagonal element given by $[\mathbf{S}_t]_{ii} = \alpha_{i,t} + \boldsymbol{\beta}_{i,t}^\intercal \mathbf{Y}_t$ with $\alpha_{i,t} \in \mathbb{R}$ and $\boldsymbol{\beta}_{i,t} \in \mathbb{R}^2$ being deterministic functions of t;
- $\mathbf{J}_{i,t} = \sum_{k=1}^{N_{i,t}} \mathbf{X}_{i,k}$ for $0 \le t \le T$ is a bivariate compound Poisson process with intensity $\lambda_i > 0$ and jump-size distribution G_i defined on $\mathbb{R}^2$.

Note that, automatically, the Brownian motion $\{\mathbf{W}_t\}_{0\le t\le T}$ and the compound Poisson processes $\{\mathbf{J}_{i,t}\}_{0\le t\le T}$, $i=1,\ldots,m$, are mutually independent. See Corollary 11.5.3 of Shreve (2004) for this result or see Lemma 13.6 of Kallenberg (1997) in a more general version. A feature of this model is that it gives consideration to multiple exogenous events/shocks, realized by the bivariate compound Poisson processes $\{\mathbf{J}_{i,t}\}_{0\le t\le T}$, $i=1,\ldots,m$, which feed into all dimensions of the joint process $\{\mathbf{Y}_t\}_{0\le t\le T}$.

In the sequel, we will always assume for simplicity that certain conditions are already imposed on the coefficient functions $\mathbf{K}_t$, $\boldsymbol{\theta}_t$, $\boldsymbol{\Sigma}_t$, $\alpha_{i,t}$, $\boldsymbol{\beta}_{i,t}$, and the distributions G_i, $i=1,\ldots,m$, to ensure that the SDE (2.1) has a unique strong solution. See Theorem 1.19 of Øksendal and Sulem (2005) for a general result on this; see also Subsection 2.1 of Duffie et al. (2000) and the references therein for related discussions.

2.2 The pricing measure Q

In what follows, we introduce our structure of risk premia by following Subsection 3.1 of Duffie et al. (2000). Other closely related works include Dai and Singleton (2000), Duffee (2002), Jarrow et al. (2005), and Lando (2009).

In the terminology of Schönbucher (1998), for the diffusion risk captured by $\{\mathbf{W}_t\}_{0\le t\le T}$, the risk premium in the economy is assumed to be determined by the market price of diffusion risk

$$\boldsymbol{\Gamma}_t = \sqrt{\mathbf{S}_t}\boldsymbol{\gamma}_t, \tag{2.2}$$

where $\boldsymbol{\gamma}_t = (\gamma_{1,t},\gamma_{2,t})^\intercal \in \mathbb{R}^2$ is a bivariate deterministic functions of t. Define

$$Z_{1,t} = \exp\left\{\int_0^t \boldsymbol{\Gamma}_s^\intercal d\mathbf{W}_s - \frac{1}{2}\int_0^t \boldsymbol{\Gamma}_s^\intercal\boldsymbol{\Gamma}_s ds\right\}, \qquad 0\le t\le T. \tag{2.3}$$

We assume that the process $\{\boldsymbol{\Gamma}_t\}_{0\le t\le T}$ satisfies a certain integrability condition so that $\{Z_{1,t}\}_{0\le t\le T}$ is a martingale under P.

Define

$$d\mathbf{W}_t^Q = d\mathbf{W}_t - \boldsymbol{\Gamma}_t dt, \qquad 0\le t\le T, \tag{2.4}$$

which we will show later is a standard bivariate Brownian motion under the measure Q we construct. Then rewrite $d\mathbf{Y}_t$ as

$$\begin{aligned} d\mathbf{Y}_t &= \mathbf{K}_t(\boldsymbol{\theta}_t - \mathbf{Y}_t)dt + \boldsymbol{\Sigma}_t\sqrt{\mathbf{S}_t}\left(d\mathbf{W}_t^Q + \sqrt{\mathbf{S}_t}\boldsymbol{\gamma}_t dt\right) + \sum_{i=1}^m d\mathbf{J}_{i,t} \\ &= \mathbf{K}_t^*(\boldsymbol{\theta}_t^* - \mathbf{Y}_t)dt + \boldsymbol{\Sigma}_t\sqrt{\mathbf{S}_t}d\mathbf{W}_t^Q + \sum_{i=1}^m d\mathbf{J}_{i,t}, \end{aligned}$$

where $\mathbf{K}_t^* = \mathbf{K}_t - \boldsymbol{\Sigma}_t\boldsymbol{\Phi}_t$, $\boldsymbol{\theta}_t^* = (\mathbf{K}_t^*)^{-1}(\mathbf{K}_t\boldsymbol{\theta}_t + \boldsymbol{\Sigma}_t\boldsymbol{\psi}_t)$, the ith row of $\boldsymbol{\Phi}_t \in \mathbb{R}^{2\times 2}$ is given by $\gamma_{i,t}\boldsymbol{\beta}_{i,t}^\intercal$, and $\boldsymbol{\psi}_t = (\gamma_{1,t}\alpha_{1,t},\gamma_{2,t}\alpha_{2,t})^\intercal \in \mathbb{R}^2$.

The jump part in (2.1) consists of multiple independent compound Poisson processes under P. When introducing the market price of jump risk, we consider both the jump-frequency risk and the jump-size risk, but we still restrict our study to structure-preserving equivalent changes of measures, which retain the mathematical tractability of the model. Mimicking Proposition 9.6 of Cont and Tankov (2004), we perform a change of measure but require that under the changed measure $\{\mathbf{J}_{i,t}\}_{0\le t\le T}$, $i = 1, \ldots, m$, remain to be independent compound Poisson processes. To be precise, for each i, we change the intensity from λ_i to $\lambda_i^* > 0$, with the ratio $\chi_i = \frac{\lambda_i^*}{\lambda_i} > 0$ reflecting the market price of jump-frequency risk. Also, we change the common jump-size distribution from G_i to G_i^* which shares the support of G_i. Denote by $D_i \subset \mathbb{R}^2$ the common support of G_i and G_i^*. By the Radon–Nikodym theorem, there is a positive measurable function $g_i(\mathbf{x})$ such that

$$\frac{dG_i^*}{dG_i}(\mathbf{x}) = g_i(\mathbf{x}), \qquad \mathbf{x} \in D_i, \tag{2.5}$$

in which the market price of jump-size risk is embedded. Then define

$$Z_{2,t} = \prod_{i=1}^{m} e^{-(\lambda_i^* - \lambda_i)t} \prod_{k=1}^{N_{i,t}} \left(\frac{\lambda_i^*}{\lambda_i} g_i\left(\mathbf{X}_{i,k}\right) \right), \qquad 0 \le t \le T, \tag{2.6}$$

which is a martingale under P.

Building on (2.3) and (2.6), we define the pricing measure Q by

$$\frac{dQ}{dP} = Z_{1,T} Z_{2,T}. \tag{2.7}$$

Proposition 2.1 below, the proof of which is postponed to Appendix A.1, shows that the AJD structure is preserved under the pricing measure Q:[5]

Proposition 2.1 *Under the pricing measure Q,*

- $\{\mathbf{W}_t^Q\}_{0\le t\le T}$ *defined by* (2.4) *is a standard bivariate Brownian motion;*
- *for each $i = 1, \ldots, m$, $\{\mathbf{J}_{i,t}\}_{0\le t\le T}$ is a bivariate compound Poisson process with intensity λ_i^* and common jump-size distribution G_i^*;*
- $\{\mathbf{W}_t^Q\}_{0\le t\le T}$ *and* $\{\mathbf{J}_{i,t}\}_{0\le t\le T}$, $i = 1, \ldots, m$, *are mutually independent.*

[5]Note that our construction of the Radon–Nikodym derivative and hence the equivalent martingale measure Q is restricted to a finite-time horizon. While this suffices for our study, we would like to point out that the extension to the infinite-time horizon, which is needed when pricing, e.g., perpetuities, is not straightforward. Following the martingale convergence theorem, a sufficient condition to ensure the existence of an equivalent martingale measure Q on $\mathcal{F}$ is that the constructed Radon–Nikodym derivatives $Z_T = \frac{dQ_T}{dP_T}$, $0 \le T \le \infty$, are uniformly integrable under P; see, e.g., Theorem I.10 of Protter (2005). This however does not hold in general in the current context. See Example 7.3 of Klebaner (2012) for a special case. For the infinite-time horizon, the construction of an equivalent martingale measure Q on $\mathcal{F} = \bigcup_{t>0} \mathcal{F}_t$ can be found in, for example, Björk et al. (1997). Provided the existence of this Q, Theorem III.3.4 of Jacod and Shiryaev (2003) shows that there exists a P martingale density $\{Z_t\}_{0\le t\le T}$ such that $dQ_t = Z_t dP_t$ for all $0 \le t \le T$, where P_t and Q_t are the restrictions of P and Q on $\mathcal{F}_t$, respectively.

2.3 An important special case

Now consider an important special case in which the dynamics, under the P measure, of the interest rate process and the excess mortality process are modeled by

$$\begin{cases} dr_t = (m_1 - d_1 r_t)dt + \sigma_1 dW_{1,t} + d\sum_{i=1}^{N_t} X_{1,i}, \\ d\mu_t = (m_2 - d_2\mu_t)dt + \sigma_2\left(\rho_1 dW_{1,t} + \sqrt{1-\rho_1^2}dW_{2,t}\right) + d\sum_{i=1}^{N_t} X_{2,i}, \end{cases} \tag{2.8}$$

where, under P,

- $m_i \in \mathbb{R}$, $d_i \neq 0$, $\sigma_i > 0$, for $i = 1, 2$, and $\rho_1 \in [-1, 1]$ are constants;
- $\{(W_{1,t}, W_{2,t})\}_{0\leq t\leq T}$ is a standard bivariate Brownian motion;
- $\{N_t\}_{0\leq t\leq T}$ is a Poisson process with intensity $\lambda > 0$;
- $\{\mathbf{X}_j = (X_{1,j}, X_{2,j})^\intercal\}_{j\in\mathbb{N}}$ is a sequence of independent and identically distributed (i.i.d.) bivariate random vectors such that the generic vector $\mathbf{X}$ is normally distributed with marginal means ν_1 and ν_2, standard deviations ϕ_1 and ϕ_2, and correlation coefficient ρ_2, denoted by $\mathbf{X} \sim N(\nu_1, \nu_2; \phi_1, \phi_2; \rho_2)$;
- $\{N_t\}_{0\leq t\leq T}$ and $\{\mathbf{X}_j\}_{j\in\mathbb{N}}$ are independent.

Note that the model captures the dependence between the interest rate and excess mortality via the diffusion correlation ρ_1, the jumps that occur jointly, and the jump correlation ρ_2.

Rewritten in the form of (2.1), the joint dynamics for $\{\mathbf{Y}_t = (r_t, \mu_t)^\intercal\}_{0\leq t\leq T}$ is

$$d\mathbf{Y}_t = \mathbf{K}_t(\boldsymbol{\theta}_t - \mathbf{Y}_t)dt + \boldsymbol{\Sigma}_t d\mathbf{W}_t + d\sum_{i=1}^{N_t}\mathbf{X}_i,$$

with

$$\mathbf{K}_t = \begin{pmatrix} d_1 & 0 \\ 0 & d_2 \end{pmatrix}, \qquad \boldsymbol{\theta}_t = \begin{pmatrix} \frac{m_1}{d_1} \\ \frac{m_2}{d_2} \end{pmatrix}, \qquad \boldsymbol{\Sigma}_t = \begin{pmatrix} \sigma_1 & 0 \\ \sigma_2\rho_1 & \sigma_2\sqrt{1-\rho_1^2} \end{pmatrix}.$$

For the latter use, let us take a look at the instantaneous correlation between r_t and μ_t. Note that

$$\begin{aligned} Cov(dr_t, d\mu_t) &= E\left[(dr_t - E[dr_t])\,(d\mu_t - E[d\mu_t])\right] \\ &= E\left[\rho_1\sigma_1\sigma_2 dt + d\sum_{i=1}^{N_t} X_{1,i}X_{2,i}\right] \\ &= \rho_1\sigma_1\sigma_2 dt + \lambda(\rho_2\phi_1\phi_2 + \nu_1\nu_2)dt. \end{aligned}$$

Similarly,

$$Var(dr_t) = \sigma_1^2 dt + \lambda(\phi_1^2 + \nu_1^2)dt, \qquad Var(d\mu_t) = \sigma_2^2 dt + \lambda(\phi_2^2 + \nu_2^2)dt.$$

The instantaneous correlation between r_t and μ_t is

$$Corr(dr_t, d\mu_t) = \frac{\rho_1\sigma_1\sigma_2 + \lambda(\rho_2\phi_1\phi_2 + \nu_1\nu_2)}{\sqrt{(\sigma_1^2 + \lambda(\phi_1^2 + \nu_1^2))\,(\sigma_2^2 + \lambda(\phi_2^2 + \nu_2^2))}}. \tag{2.9}$$

Now we look at the Q version of this special case. We take the simplest choice for the market price of diffusion risk (2.2) that $\mathbf{\Gamma}_t = (\gamma_1, \gamma_2)^\intercal \in \mathbb{R}^2$. Then with $dW_{i,t} = dW_{i,t}^Q + \gamma_i dt$ for $i = 1, 2$, we can rewrite the dynamics as

$$\begin{cases} dr_t = (m_1^* - d_1 r_t)dt + \sigma_1 dW_{1,t}^Q + d\sum_{i=1}^{N_t} X_{1,i}, \\ d\mu_t = (m_2^* - d_2\mu_t)\,dt + \sigma_2\left(\rho_1 dW_{1,t}^Q + \sqrt{1-\rho_1^2}dW_{2,t}^Q\right) + d\sum_{i=1}^{N_t} X_{2,i}, \end{cases} \tag{2.10}$$

with

$$m_1^* = m_1 + \gamma_1\sigma_1, \qquad m_2^* = m_2 + \gamma_1\sigma_2\rho_1 + \gamma_2\sigma_2\sqrt{1-\rho_1^2}.$$

We follow Subsection 2.2 to specify the market prices of the jump-frequency risk and jump-size risk. In summary, we have the following, under Q:

- $\{(W_{1,t}^Q, W_{2,t}^Q)\}_{0\le t\le T}$ is a standard bivariate Brownian motion;
- $\{N_t\}_{0\le t\le T}$ is a Poisson process with intensity $\lambda^* > 0$, with the ratio $\chi = \frac{\lambda^*}{\lambda} > 0$ reflecting the market price of jump-frequency risk;
- $\{\mathbf{X}_j\}_{j\in\mathbb{N}}$ is a sequence of i.i.d. bivariate random vectors with common distribution function G^* on $\mathbb{R}^2$;
- $\{N_t\}_{0\le t\le T}$ and $\{\mathbf{X}_j\}_{j\in\mathbb{N}}$ are independent.

Example 2.1 Now we employ the normalized multivariate exponential tilting to construct the common distribution G^* of $\{\mathbf{X}_j\}_{j\in\mathbb{N}}$ under Q. See Section 5 of Wang (2007) for more details about this distortion approach; see also Cox et al. (2006) and Lin et al. (2013), who apply this approach, in a somewhat simplified situation, to price mortality/longevity linked securities.

Assume that under P, the generic vector $\mathbf{X} = (X_1, X_2)^\intercal$ is bivariate normal with marginal means ν_1 and ν_2, standard deviations ϕ_1 and ϕ_2, and correlation coefficient ρ_2, as specified before. Let the market prices of jump-size risk be κ_1 and κ_2, respectively. Then the common distribution G^* is constructed by specifying the measurable function (2.5) to

$$\frac{dG^*}{dG}(\mathbf{x}) = g(\mathbf{x}) = \varphi E\left[\exp\left\{\sum_{k=1}^{2}\eta_k V_k\right\}\middle|\,\mathbf{X} = \mathbf{x}\right], \qquad \mathbf{x}\in\mathbb{R}^2,$$

where

- the vector (X_1, X_2, V_1, V_2) is jointly normal with V_1 and V_2, called the reference variables, specified to be standard normal for simplicity;
- the constants η_1 and η_2 satisfy $\kappa_i = -\sum_{j=1}^{2}\hat{\rho}_{i,j}\eta_j$, $i = 1, 2$, with each $\hat{\rho}_{i,j}$ being the correlation of X_i and V_j;

- φ is a normalizing constant to ensure that $g(\mathbf{x})$ is a proper Radon–Nikodym derivative over $\mathbb{R}^2$.

It is easy to see that under Q the vector $\mathbf{X}$ remains bivariate normal with marginal means $\nu_1^* = \nu_1 + \phi_1\kappa_1$ and $\nu_2^* = \nu_2 + \phi_2\kappa_2$, standard deviations ϕ_1 and ϕ_2, and correlation coefficient ρ_2; that is, only the marginal means are changed.

In this case, the Radon–Nikodym derivative (2.7) is explicated as

$$\begin{aligned}\frac{dQ}{dP} &= \exp\left\{\gamma_1 W_{1,T} + \gamma_2 W_{2,T} - \frac{1}{2}\left(\gamma_1^2 + \gamma_2^2\right)T - (\lambda^* - \lambda)T\right\}\prod_{k=1}^{N_T}\left(\frac{\lambda^*}{\lambda}g\left(\mathbf{X}_k\right)\right)\\ &= \exp\left\{\gamma_1 W_{1,T} + \gamma_2 W_{2,T} - \frac{1}{2}\left(\gamma_1^2 + \gamma_2^2\right)T - \lambda(\chi - 1)T\right\}\chi^{N_T}\prod_{k=1}^{N_T} g\left(\mathbf{X}_k\right). \qquad (2.11)\end{aligned}$$

3 Modeling mortality-linked securities

Consider a general structure of an MLS, which makes payments at time points

$$0 < t_1 < t_2 < \cdots < t_n = T < \infty,$$

where 0 and T represent the issuance date and the maturity date, respectively. Each payment ξ_{t_k} made at time t_k is linked to a certain mortality index. Technically, for each $k = 1, \ldots, n$, we assume that ξ_{t_k} is measurable with respect to $\mathcal{F}_{t_k}^2$. Given the pricing measure Q specified in Section 2, the risk-neutral price of this MLS is

$$P_t = E_t^Q\left[\sum_{t<t_k\le T}\exp\left\{-\int_t^{t_k} r_s ds\right\}\xi_{t_k}\right], \qquad 0 \le t < T. \qquad (3.1)$$

We use the following examples to illustrate the wide applicability of our pricing framework. As one of the simplest cases, the first example makes a connection of our framework to the CoRI Retirement Indexes.

Example 3.1 The CoRI Retirement Indexes are introduced by BlackRock to help determine, in today's dollars, the estimated cost of purchasing lifetime retirement income at age 65 or later for 20 cohorts in the US.[6] This lifetime income includes \$1 annual inflation-adjusted payments from the retirement age $T' = 65$ until age $T = 115$, where the maximum age is fixed to 115 under the belief that no one will survive beyond this age. We consider a specific cohort i aged $x + t$ at time t. When applying the pricing formula (3.1) to compute the CoRI Index $I_t^{i,x}$ at time t, it is important to keep in mind the following. First, to match the annual inflation-adjusted payments, a real interest rate $\{r_s\}_{t\le s\le T}$ that removes the effects of inflation should be used to discount the cash flows. Second, the \$1 annual

[6]See more details at `https://www.blackrock.com/cori-retirement-income-planning/literature/whitepaper/cori-index-whitepaper-revised.pdf`.

payments are contingent on the survival of a representing individual whose mortality rate follows $\{\mu_s^{i,x}\}_{t\le s\le T}$. To capture this contingency, when computing $I_t^{i,x}$, the annual payments need to be adjusted to

$$\xi_{t_k} = \begin{cases} 0, & t_k \le T' - x, \\ \exp\left\{-\int_t^{t_k} \mu_s^{i,x} ds\right\}, & T' - x < t_k \le T - x. \end{cases}$$

Putting together, by (3.1) we have

$$I_t^{i,x} = E_t^Q \left[\sum_{\max\{t, T'-x\} < t_k \le T-x} \exp\left\{-\int_t^{t_k} \left(r_s + \mu_s^{i,x}\right) ds\right\} \right],$$

which is similar to Proposition 5.1 of Biffis (2005) and formula (14) of Xu et al. (2020).

Next, we consider a more sophisticated longevity/mortality trend bond, with the Swiss Re Kortis bond as a prototype, which is understood to be useful to hedge systematic longevity/mortality risk.

Example 3.2 In this bond, the payoff is linked to the associated divergence index (DI) that is used to quantify the discrepancy between the mortality trends of two or multiple populations. Suppose a principal K at the issuance date 0. Using the DI as the trigger, assume the attachment level a and the exhaustion level b for $1 < a < b < \infty$. At any time $t \le T$, if the bond is triggered, that is, $\mathrm{DI}_t > a$, then the bond is depreciated accordingly, for which case following (4) of Hunt and Blake (2015) or (2.4) of Li and Tang (2019) we introduce the principal reduction factor (PRF) equal to

$$\mathrm{PRF}_t = \frac{(\mathrm{DI}_t - a)_+ - (\mathrm{DI}_t - b)_+}{b - a}.$$

Thus, the remaining principal at maturity is

$$\begin{aligned} D &= K\left(1 - \sum_{0<t_k\le T} \mathrm{PRF}_{t_k}\right)_+ \\ &\approx K\left(1 - \max_{0<t_k\le T} \mathrm{PRF}_{t_k}\right) \\ &= K\left(1 - \frac{(\mathrm{DI}^* - a)_+ - (\mathrm{DI}^* - b)_+}{b - a}\right), \end{aligned}$$

where $\mathrm{DI}^* = \max_{0<t_k\le T} \mathrm{DI}_{t_k}$, and the approximation is justified by the reasoning that the probability of having two or more mortality catastrophes within the risk period $[0, T)$ is negligible. Without going into its detailed structure, we denote by C_{t_k} the coupon payment for the period of $(t_{k-1}, t_k]$, where $t_0 = 0$. The coupon C_{t_k} may be linked to the varying

principal of the bond, or, for simplicity, set to be $C_{t_k} = cK(t_k - t_{k-1})$ for some constant coupon rate c. In this example, we have

$$\begin{cases} \xi_{t_k} = C_{t_k}, & 0 < t_k < T, \\ \xi_T = C_T + D. \end{cases}$$

Then the pricing formula (3.1) becomes applicable.

Our last and working example in this paper is a hypothetical bond which closely resembles the Atlas bond. In September 2013, the Atlas IX Capital launched a CAT bond to provide extreme mortality protection.[7] The risk period was from 1 January 2013 to 31 December 2018 and the bond received a class B - 'BB' rating from Standard and Poor's. The PRF of the Atlas bond is determined by an underlying mortality index which represents the age- and gender-weighted death probability across the US. Initially, there were two tranches offered, Class A notes with lower risk and Class B notes with higher risk. In fact, the Class A notes was pulled out from the market due to lack of demand. Nevertheless, Class B notes were marketed at US$50m but ended up at US$180m in size, indicating a strong risk appetite of investors in the market. The Class B tranche had an attachment probability of 1.16% and exhaustion probability of 0.74%. The expected loss of the Atlas bond was 0.92% and the coupon rate was 3.25%.

The constructed hypothetical bond is described as follows:

Example 3.3 Denote by $t_0 = 0$ the bond issuance date 30 September 2013, by K the bond principal, and thus the bond maturity date 31 December 2018 is $T = 5\frac{1}{4}$. Suppose an annual coupon rate of $c = 3.25\%$ payable quarterly. Thus, we have 21 coupon dates, with the first coupon date $t_1 = \frac{1}{4}$ corresponding to 31 December 2013, the second coupon date $t_2 = \frac{2}{4}$ corresponding to 30 March 2014, and so on, until the last coupon date, also the maturity date, $t_{21} = T = 5\frac{1}{4}$, corresponding to 31 December 2018.

Suppose an attachment point a and an exhaustion point b are determined based on a given dataset, with $0 < a < b < \infty$. As in Example 3.2, if the bond is triggered by time T, that is, if $\mu^* = \max_{0<t_k\leq T} \mu_{t_k} > a$, then with the PRF defined to be

$$\text{PRF} = \frac{(\mu^* - a)_+ - (\mu^* - b)_+}{b - a},$$

the remaining principal at maturity is

$$D = K\left(1 - \frac{(\mu^* - a)_+ - (\mu^* - b)_+}{b - a}\right).$$

Recall the constant coupon rate c assumed at the beginning. Putting together, we have the payoff structure

$$\begin{cases} \xi_{t_k} = \frac{c}{4}K, & 0 < t_k < T, \\ \xi_T = \frac{c}{4}K + D. \end{cases}$$

[7] For more details of the deal, please refer to `https://www.artemis.bm/deal-directory/atlas-ix-capital-limited-series-2013-1`.

The (full) price, with accrued interest included, of the bond at time $0 \leq t \leq T$ is

$$P_t = \frac{c}{4} K \sum_{t<t_k \leq T} P(t, t_k) + KP(t, T) - KE_t^Q \left[e^{-\int_t^T r_s ds} \frac{(\mu^* - a)_+ - (\mu^* - b)_+}{b - a} \right], \tag{3.2}$$

where $P(t, s)$, for $0 \leq t \leq s < \infty$, is the time t price of a risk-free zero-coupon bond with maturity date s.

4 Empirical studies

4.1 Data description

Our empirical studies focus on the US experience. To calibrate the bivariate AJD model described in Section 2.3, we consider the US weekly mortality and interest rate data for the period of 2017–2020, which are collected from three sources as follows:

CDC COVID-19 Death Data. In response to the COVID-19 pandemic, the CDC is providing weekly updates on national estimates of excess deaths to reflect the burden of mortality potentially associated with the pandemic.[8] This excess death dataset is available from January 2017 onwards. We collect national-level weekly observed deaths and the expected deaths for the period January 2017 – January 2021.

CDC WONDER Database. The CDC WONDER online database provides a rich query system for the analysis of public health data and vital statistics. We collect population data for 2017–2019 via the online query "Bridged-Race Population Estimates 1990–2019 Request", and collect the population estimate for 2020 via the online query "National Population Projections 2014–2060 Request".

Federal Reserve Economic Data (FRED). The weekly interest rate data comes from the 3-month treasury bill rates, collected at the same frequency and for the same period as the mortality data.

As we focus on extreme mortality experience, instead of mortality rate, we choose to examine excess mortality defined as

$$\mu_t = \frac{d_t - E(d_t)}{e_t} \times 100,$$

where d_t is the observed number of deaths during a time period ending at t, and $E(d_t)$ and e_t are, respectively, the expected number of deaths and the population exposure for the same period. While the excess mortality in the literature is usually defined through death counts per annum, the more granular mortality data allows for a more refined definition based on weekly death counts. Since weekly population exposures are unavailable, for simplicity, we approximate them based on the annual population data assuming equal exposures across weeks in a calendar year.

[8] For more information, please refer to `https://www.cdc.gov/nchs/nvss/vsrr/covid19/excess_deaths.htm`.

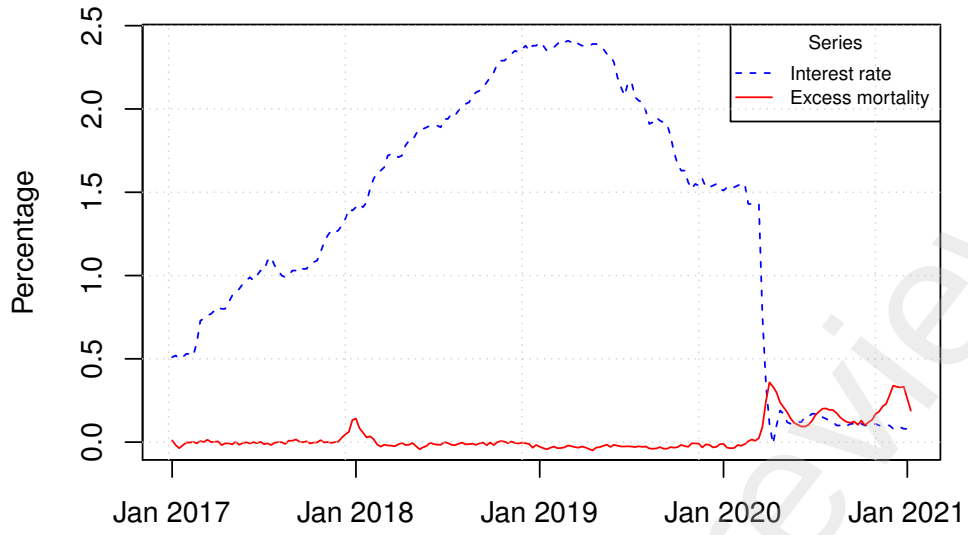

Figure 4.1. This figure plots weekly interest rate and excess mortality for the US. Note that from 6 March 2020, we introduce a three-week lag in the interest rate data to synchronize the first emergency rate cut by the Federal Reserve and the first observed surge in excess mortality.

As one of the most devastating global events since World War II, the COVID-19 pandemic has resulted in a substantial level of excess mortality for most countries. According to the New York Times, there were 574,000 more deaths than usual in the 12-month period from March 2020 to March 2021.[9] To combat the COVID-19 pandemic, on 3 March 2020, the Federal Reserve cut the base rate by 50 basis points. As the COVID-19 fear grew, on 15 March 2020, the Federal Reserve further cut the base rate down to near zero. Obviously, the "higher than usual" mortality rate and the "lower than usual" interest rate are not a coincidence, but both resulted from the shock imposed by the COVID-19 pandemic. However, it should be noted that only toward the end of March did the national death tolls start to climb, which then led to a sharp increase in excess mortality. Although the jumps in interest rate and excess mortality came from the same source, there was a time lag in the responses of the two processes. In other words, the Federal Reserve proactively adjusted its monetary policy, foreseeing the devastating impacts of COVID-19 on population health and the economy. To reflect upon this, we argue that from the week ending 6 March 2020, a three-week lag in the interest rate data should be introduced to synchronize the first emergency rate cut by the Federal Reserve and the first observed surge in excess mortality. The adjusted series are shown in Figure 4.1.

[9]See full news article at `https://www.nytimes.com/interactive/2021/01/14/us/covid-19-death-toll.html`.

4.2 Model calibration including the pandemic experience

We first fit the AJD model (2.8) introduced in Section 2.3 to the entire dataset from 2017–2020, particularly including the COVID-19 pandemic experience. We adopt the likelihood inference methodology proposed by Pienaar and Varughese (2016), where parameter estimation is performed under the MCMC algorithm implemented via R package `DiffusionRjgqd`. Table 4.1 presents the estimated parameter values, as well as their corresponding 95% confidence intervals (CIs). The convergence diagnostics for the MCMC sampler, as well as the autocorrelation function (ACF) of MCMC draws, are plotted in Figures A.1 and A.2 in the Appendix.

	Estimate	Lower CI	Upper CI
d_1	0.126	−0.123	0.407
m_1	0.005	0.001	0.009
σ_1	0.002	0.002	0.003
d_2	2.301	0.656	4.357
m_2	0.002	−0.126	0.100
σ_2	0.124	0.109	0.147
ρ_1	−0.038	−0.101	0.022
λ	4.865	1.820	8.572
ν_1	−0.001	−0.002	0.000
ν_2	0.035	0.001	0.088
ϕ_1	0.002	0.001	0.004
ϕ_2	0.074	0.049	0.114
ρ_2	−0.479	−0.767	−0.065

Table 4.1. Estimated parameters for model (2.8) based on data including the pandemic experience, from 2017 to 2020.

The calibrated dynamics of the interest rate process and the excess mortality process are

$$\begin{cases} dr_t = (0.005 - 0.126 r_t)dt + 0.002 dW_{1,t} + d\sum_{i=1}^{N_t} X_{1,i}, \\ d\mu_t = (0.002 - 2.301\mu_t)dt + 0.124\,(-0.038 dW_{1,t} + 0.99928 dW_{2,t}) + d\sum_{i=1}^{N_t} X_{2,i}, \end{cases} \tag{4.1}$$

where, under P,

- $\{(W_{1,t}, W_{2,t})\}_{0\le t\le T}$ is a standard bivariate Brownian motion;
- $\{N_t\}_{0\le t\le T}$ is a Poisson process with intensity 4.865;
- $\{\mathbf{X}_j = (X_{1,j}, X_{2,j})^\intercal\}_{j\in\mathbb{N}}$ is a sequence of i.i.d. bivariate random vectors such that the generic vector $\mathbf{X}$ is normally distributed with marginal means −0.001 and 0.035, standard deviations 0.002 and 0.074, and correlation coefficient −0.479, that is, $\mathbf{X} \sim N(-0.001, 0.035; 0.002, 0.074; -0.479)$;

Using the data, we detect joint jumps with an estimated intensity of 4.865 per year. Moreover, we find a strong negative jump correlation of $\rho_2 = -0.479$, which means that the excess mortality and interest rate tend to jump in the opposite directions. On the other hand, the two diffusions are nearly independent, with an estimated diffusion correlation of $\rho_1 = -0.038$. Plugging these calibrated values into (2.9), we obtain the instantaneous correlation

$$Corr(dr_t, d\mu_t) = -0.450.$$

In the proposed AJD model, diffusions represent market fluctuations in their normal range, while jumps are used to capture unusual changes that often result from catastrophic events. Based on the values of ρ_1 and ρ_2, as well as the instantaneous correlation calculated above, we find that the significant instantaneous correlation here is mainly caused by the joint jumps. Therefore, under extreme market conditions driven by catastrophes or shocks, the independence assumption is no longer appropriate and can become fundamentally wrong.

4.3 Model calibration excluding the pandemic experience

We now fit model (2.8) to pre-pandemic data only, from 2017 to 2019. The estimated parameters and their 95% CIs are shown in Table 4.2. The convergence diagnostics for the MCMC sampler and the ACF of MCMC draws are presented in Figures A.3 and A.4.

	Estimate	Lower CI	Upper CI
d_1	0.727	0.222	1.181
m_1	0.016	0.006	0.024
σ_1	0.002	0.002	0.003
d_2	16.368	9.015	23.134
m_2	−0.217	−0.349	−0.094
σ_2	0.095	0.086	0.105
ρ_1	0.017	−0.049	0.088
λ	1.909	0.497	3.780
ν_1	0.000	−0.001	0.001
ν_2	0.026	0.001	0.058
ϕ_1	0.001	0.000	0.003
ϕ_2	0.056	0.041	0.072
ρ_2	−0.475	−0.558	−0.384

Table 4.2. Estimated parameters for model (2.8) based on data excluding the pandemic experience, from 2017 to 2019.

The calibrated dynamics of the interest rate process and the excess mortality process are

$$\begin{cases} dr_t = (0.016 - 0.727 r_t)dt + 0.002 dW_{1,t} + d\sum_{i=1}^{N_t} X_{1,i}, \\ d\mu_t = (-0.217 - 16.368\mu_t)dt + 0.095\,(0.017 dW_{1,t} + 0.99986 dW_{2,t}) + d\sum_{i=1}^{N_t} X_{2,i}, \end{cases} \tag{4.2}$$

where, under P,

- $\{(W_{1,t}, W_{2,t})\}_{0\le t\le T}$ is a standard bivariate Brownian motion;
- $\{N_t\}_{0\le t\le T}$ is a Poisson process with intensity 1.909;
- $\{\mathbf{X}_j = (X_{1,j}, X_{2,j})^\intercal\}_{j\in\mathbb{N}}$ is a sequence of i.i.d. bivariate random vectors such that the generic vector $\mathbf{X}$ is normally distributed with marginal means 0.000 and 0.026, standard deviations 0.001 and 0.056, and correlation coefficient -0.479, that is, $\mathbf{X} \sim N(0.000, 0.026; 0.001, 0.056; -0.479)$;

We again find a strong negative jump correlation of $\rho_2 = -0.475$ and that the two diffusions can still be seen as independent, with $\rho_1 = 0.017$. However, the estimates of some parameters have changed notably compared to those in Table 4.1. In particular, joint jumps are detected with a much lower frequency at $\lambda = 1.909$ per year, and the means and variances of jump sizes tend to be smaller for both the interest rate and excess mortality. Plugging the calibrated values in Table 4.2 into (2.9), we obtain

$$Corr(dr_t, d\mu_t) = -0.153.$$

That is, due to the less frequent joint jumps, the dependence between the interest rate and excess mortality is much weaker—but still significant—in the pre-pandemic world. Moreover, some easy calculations show that the changes result in a substantial increase of the long-term average excess mortality from -0.010 pre-pandemic to 0.075 post-pandemic.

5 Implied market prices of risk

Understanding the MPRs is an important step toward understanding the mortality risk market and how it may react to a pandemic experience. Since precise calibration of the implied MPRs is challenging due to lack of data on relevant market deals, we compute the MPRs based on the hypothetical bond designed in Example 3.3. In doing so, we accept the assumption that the hypothetical bond, if issued on 30 September 2013 under the then market conditions, would have been traded at the same prices as the Atlas bond. This assumption is largely innocuous, since the hypothetical bond closely resembles the Atlas bond in structure, covers the same population, and shares the same attachment and exhaustion probabilities.

The price data used for our calibration is obtained from the Lane Financial L.L.C. annual reviews of the catastrophe insurance market, which include quarter-end indicative secondary market prices of various catastrophe-linked securities. The 2014–2019 reviews, which cover the tenor of the Atlas bond, list the average spreads for the bond indicated by the dealers in the market.

Our secondary market price data contains 21 quarterly observations of market-indicated spreads during the period of September 2013 – September 2018, which we denote by $c^*_{t_k}$, $t_k = \frac{k}{4}$, $k = 0, 1, \ldots, 20$. We illustrate these spreads in Figure 5.1.

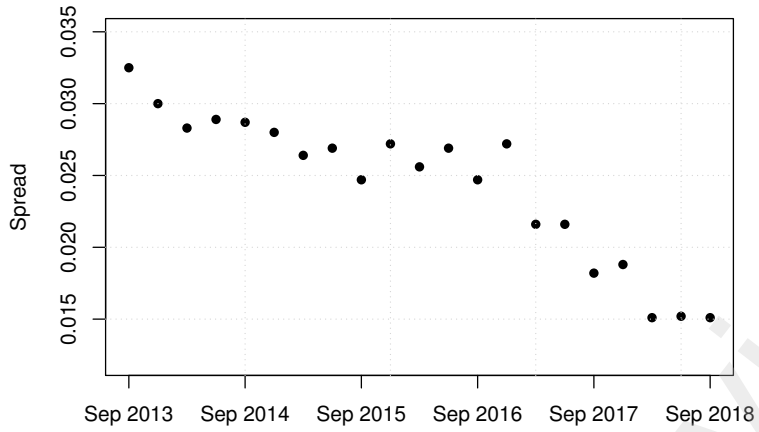

Figure 5.1. This figure plots the quarterly market-indicated spreads of the Atlas bond from September 2013 to September 2018 inclusive, published by Lane Financial L.L.C.

Note that the bond price at each time point t_k depends on the level of interest rate and excess mortality at that time. While the interest rate data is available, the excess deaths information from the CDC does not date back to September 2013. Therefore, we project excess deaths based on the information available then and via the seasonal ARIMA model proposed by Li and Tang (2021), which incorporates both non-seasonal and seasonal factors in a multiplicative model. The estimated quarterly excess mortality is shown in Figure 5.2.

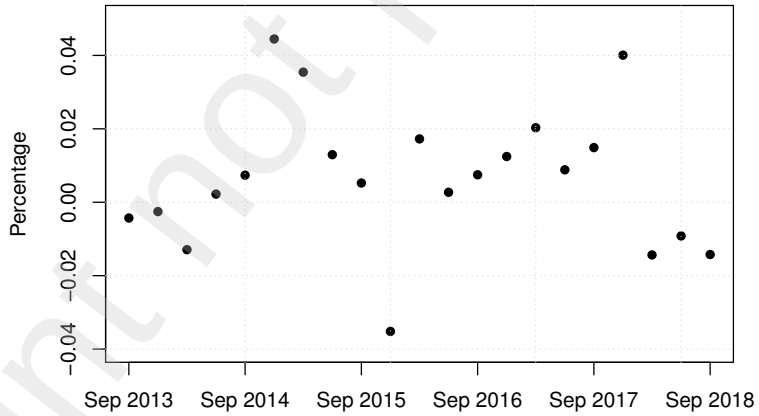

Figure 5.2. This figure shows the estimated quarterly excess mortality based on the seasonal ARIMA model.

5.1 Three scenarios

Our pricing measure Q is constructed through the Radon–Nikodym derivative (2.11) with the MPR vector $\boldsymbol{\zeta} = (\gamma_1, \gamma_2; \kappa_1, \kappa_2; \chi)$. For each $k = 0, 1, \ldots, 20$, the bond price $p^{\boldsymbol{\zeta}}_{t_k}(c^*_{t_k})$, evaluated at the spread level $c^*_{t_k}$ under Q, should be close to the par value, which we assume

to be 100 for simplicity. We calibrate the MPRs by searching for the vector $\boldsymbol{\zeta}$ that minimizes the sum squared error

$$\sum_{k=0}^{20} \left(P_{t_k}^{\boldsymbol{\zeta}} \left(c_{t_k}^* \right) - 100 \right)^2. \tag{5.1}$$

Recall model (4.1), estimated with the pandemic data, and model (4.2), estimated without it. We identify the MPRs for three different scenarios:

S1. The underlying risks follow model (4.1) and the bond trigger levels are designed according to model (4.1);

S2. The underlying risks follow model (4.2) and the bond trigger levels are designed according to model (4.2);

S3. The underlying risks follow model (4.1) but the bond trigger levels are designed according to model (4.2).

First, we consider scenario **S1**. To align the bond's attachment and exhaustion probabilities with the Atlas bond's, which are 1.16% and 0.74%, respectively, we simulate 10^6 paths of the process $\{(r_t, \mu_t)^\intercal\}_{0 \le t \le T}$ under P to estimate the exceedance probabilities for different thresholds. Figure 5.3 plots the results and suggests that to align with the Atlas bond, the attachment and exhaustion points should be 0.49 and 0.52, respectively.

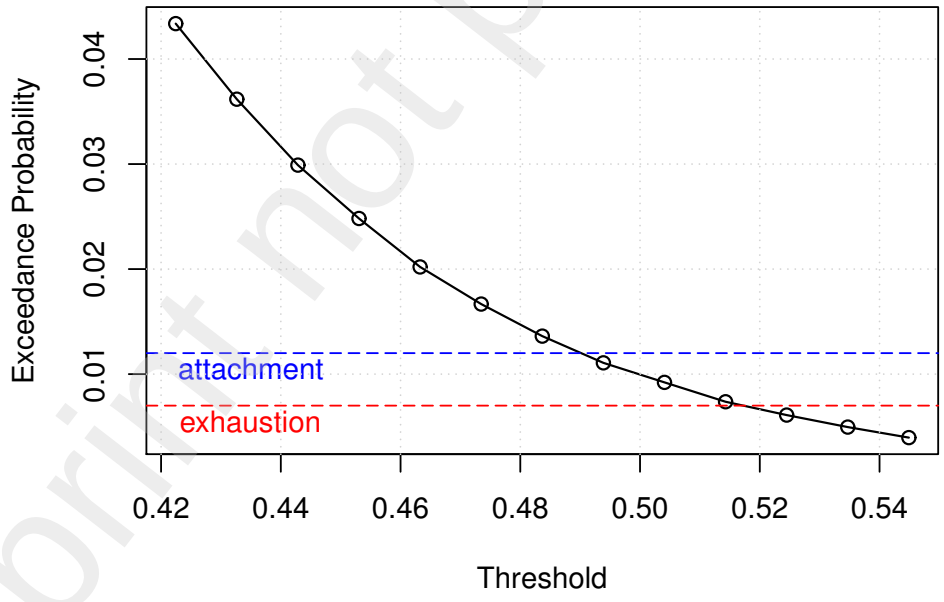

Figure 5.3. This figure shows the probability that the maximum excess mortality index during the bond tenor (μ^*, as defined in Example 3.3) exceeds a certain threshold. The probability is estimated using a simulation of 10^6 paths of the process $\{(r_t, \mu_t)^\intercal\}_{0 \le t \le T}$ under the P measure, where the process follows model (4.1).

	Scenario **S1**		Scenario **S2**		Scenario **S3**	
Parameter	Under P	Under Q	Under P	Under Q	Under P	Under Q
$m_1 \leftrightarrow m_1^*$	0.005	0.0058	0.016	0.0162	0.005	0.0072
$m_2 \leftrightarrow m_2^*$	0.002	0.0235	−0.217	−0.2080	0.002	−0.2038
$\nu_1 \leftrightarrow \nu_1^*$	−0.001	−0.0008	0.000	0.0001	−0.001	0.0011
$\nu_2 \leftrightarrow \nu_2^*$	0.035	0.0638	0.026	0.0314	0.035	−0.2673
$\lambda \leftrightarrow \lambda^*$	4.865	5.3118	1.909	2.5091	4.865	7.9877

Table 5.1. This table compares the parameter values in models (2.8) and (2.10). The parameters without $*$ are the ones in model (2.8) under P and those with $*$ are the ones in model (2.10) under Q.

Let us now use the indicative prices to derive the MPRs. In our implementation, each price appearing in (5.1) is evaluated using Monte Carlo simulation based on formula (3.2) with 10^4 paths of $\{(r_t, \mu_t)^\intercal\}_{0\le t\le T}$. The minimization of (5.1) is performed using the limited-memory Broyden–Fletcher–Goldfarb–Shanno method implemented in R. The MPR vector is obtained as

$$\boldsymbol{\zeta}_1 = (0.4161,\ 0.1897;\ 0.1119,\ 0.3889;\ 1.0918)\,. \tag{5.2}$$

Recall that the set of MPRs maps the measure P to a risk-neutral measure Q, leading to a change of parameters in the process $\{(r_t, \mu_t)^\intercal\}_{0\le t\le T}$. The comparison between the parameters under the two measures is listed in Table 5.1. We can see that, investors' perceived parameter values under Q are all higher than their counterparts under P.

Next, let us consider scenario **S2**. This scenario relates to a market where both the issuer/risk modeling agent and investors lack sufficient awareness of the pandemic risk. They design and trade the bond based on model (4.2), where the pandemic experience is not accounted for. Following the procedure for scenario **S1**, we obtain the exceedance probabilities, as shown in Figure 5.4. Note that, to maintain the same trigger probabilities, the attachment and exhaustion points should be lowered to 0.13 and 0.14, respectively. It is worth pointing out that such a bond would be triggered multiple times if traded during the COVID-19 pandemic (see Figure 5.5).

Using the same optimization algorithm, we obtain the MPR vector

$$\boldsymbol{\zeta}_2 = (0.1099,\ 0.0924;\ 0.1068,\ 0.0961;\ 1.3144)\,. \tag{5.3}$$

Again, the set of MPRs leads to a change of measure where the perceived parameter values of $\{(r_t, \mu_t)^\intercal\}_{0\le t\le T}$ are all higher under Q than their counterparts under P, as listed in Table 5.1.

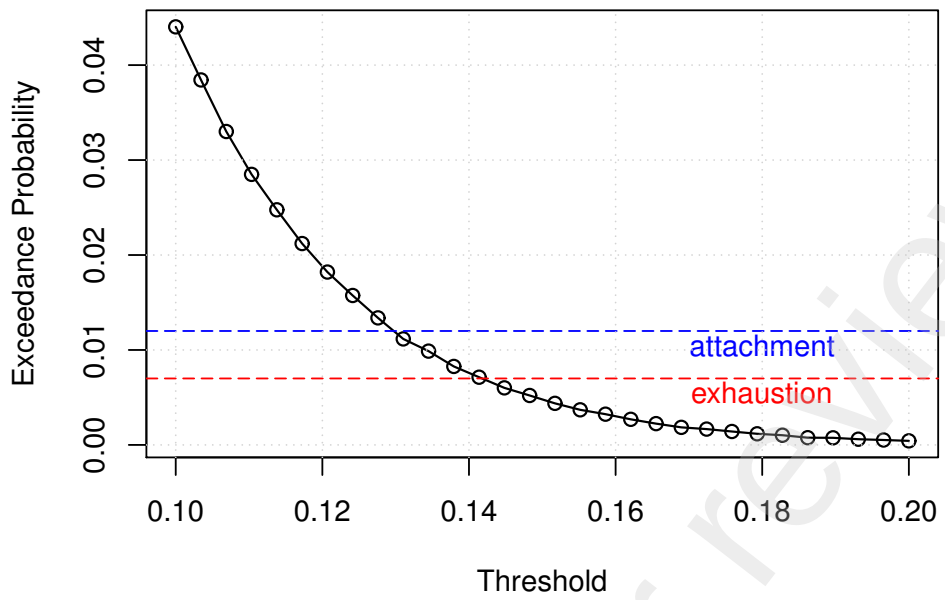

Figure 5.4. This figure shows the probability that the maximum excess mortality index during the bond tenor (μ^*, as defined in Example 3.3) exceeds a certain threshold. The probability is estimated using a simulation of 10^6 paths of the process $\{(r_t, \mu_t)^\intercal\}_{0\leq t\leq T}$ under the P measure, where the process follows model (4.2).

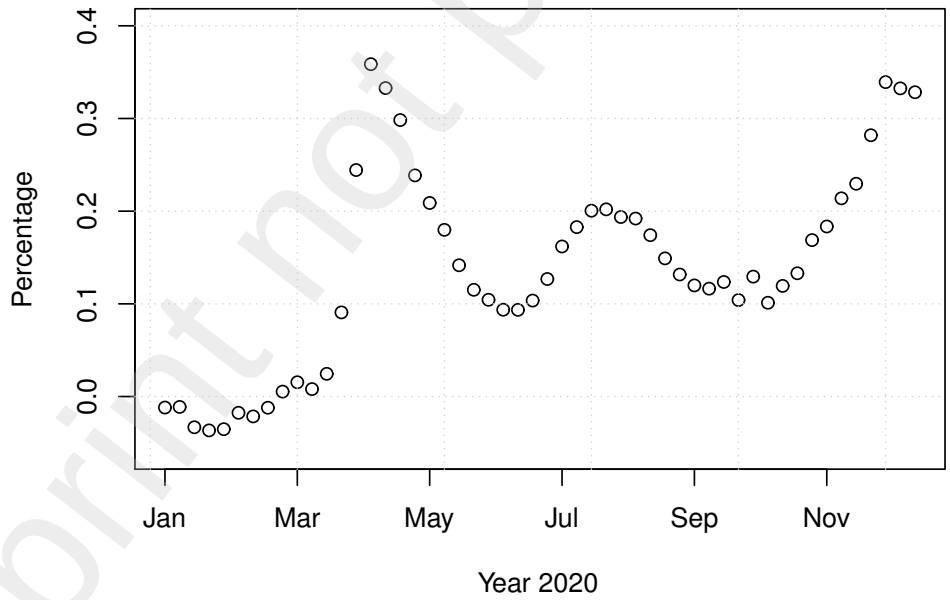

Figure 5.5. This figure plots the observed excess mortality in 2020

Last, we consider scenario **S3**. This scenario relates to the case where there is significant pandemic risk, with $\{(r_t, \mu_t)^\intercal\}_{0\leq t\leq T}$ following model (4.1), but the modeling agent and investors fail to perceive or choose to ignore the risk. They still determine the bond trigger

levels according to model (4.2) and still agree on transactions at the prices of the Atlas bond.

Following the same procedure as above to compute the MPRs yields

$$\boldsymbol{\zeta}_3 = (1.0944,\ -1.6196;\ 1.0743,\ -4.0847;\ 1.6419)\,.$$

We observe from Table 5.1 that, unlike in scenarios **S1** and **S2**, the MPRs in scenario **S3** result in some parameter values of the $\{(r_t, \mu_t)^\intercal\}_{0\le t\le T}$ process—specifically, $m_2\,(m_2^*)$ and $\nu_2\,(\nu_2^*)$—that are lower under Q than under P. This means that the investors are receiving negative mortality risk premia although the interest rate risk premia they receive are positive. Moreover, note that the negative premium on the mortality jump size is significant enough to flip the sign of the expected jump size. Therefore, a larger jump intensity perceived under Q than under P indicates that the perceived jump risk is actually lower than that under P, further contributing to the negative risk premium.

In conclusion, we have shown that turning a blind eye to potential pandemic risk—that is, failing to update the model properly for bond design to reflect the pandemic risk—could cost investors dearly.

5.2 On the post-pandemic mortality risk market

In this subsection, we aim to offer a glimpse of how a devastating pandemic experience like today's could reshape the extreme mortality risk market by, e.g., prompting industry-wide model recalibration.

We illustrate our results using a three-year hypothetical bond with coupons payable quarterly at 6% per annum, which otherwise shares the same structure as the one in Example 3.3. In this case, our pricing formula (3.2) becomes

$$P_t = 100\left(1.5\%\sum_{t<t_k\le 3} P(t,t_k) + P(t,3) - E_t^Q\left[e^{-\int_t^3 r_s ds}\frac{(\mu^*-a)_+ - (\mu^*-b)_+}{b-a}\right]\right), \quad (5.4)$$

for $0\le t\le 3$, where $t_k = \frac{k}{4}$, $k = 1,\dots,12$, and $\mu^* = \max_{0<t_k\le 3}\mu_{t_k}$.

Let us first envision a pre-pandemic world, where the modeling agent and investors believe that the underlying risks follow model (4.2), determine the trigger levels accordingly (Figure 5.4), and price the risk using the MPR vector $\boldsymbol{\zeta}_2$ in (5.3). In this case, formula (5.4) leads to a time 0 bond price of 112.6.

Now suppose that the market participants have experienced a pandemic like COVID-19, have opted for model (4.1) to describe the underlying risks, and have updated their MPR vector to $\boldsymbol{\zeta_1}$ in (5.2). By formula (5.4), the time 0 bond value is found to be 7.0. While this is an extreme example, it sheds light on a possible overhaul of the pricing mechanism due to the pandemic and the potential disruption it causes to the mortality risk market.

Note that in practice, the sponsor may modify the bond design in response to the pandemic experience by, e.g., raising its trigger levels. In our further analysis, we consider a

scenario where the attachment and exhaustion points, respectively, have been raised substantially from 0.13 and 0.14 to, for illustration purpose, 0.3 and 0.32. We now further illustrate our idea by demonstrating how the bond price reacts over time to the pandemic experience.

Recall that the bond price at any time point depends on the interest rate level then and the mortality levels until then. Therefore, to show the bond price evolutions under different scenarios, we generate several paths of $\{(r_t, \mu_t)\}_{0\le t\le 3}$ and obtain a price curve along each path. The prices on the curves are all computed based on formula (5.4) using simulation with 10^5 paths.

We present the results for the pre- and post-pandemic markets in Figures 5.6 and 5.7, respectively. The four graphs in each figure correspond to four scenarios generated for the underlying risk process, which lead to either a full return or a partial reduction of the bond principal.

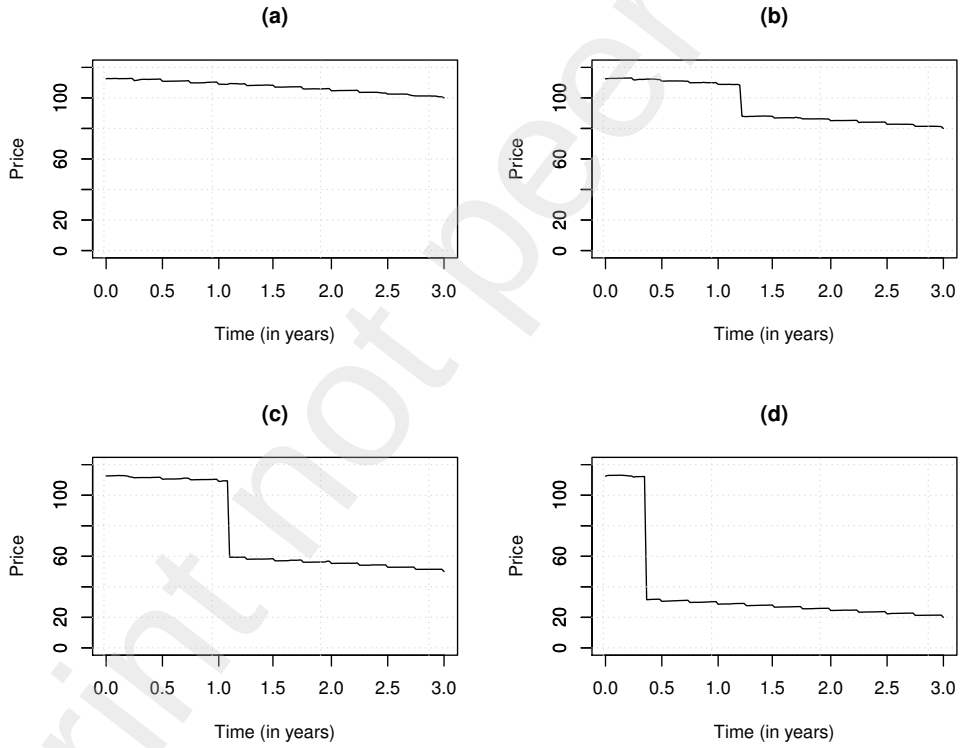

Figure 5.6. This figure shows the price evolutions for a three-year bond with coupons payable quarterly at 6% per annum and attachment and exhaustion points at 0.13 and 0.14, respectively. Each of the graphs (a)–(d) is obtained under a scenario generated for the risk process $\{(r_t, \mu_t)^\intercal\}_{0\le t\le 3}$. The prices are calculated based on formula (5.4), model (4.2), MPR vector $\boldsymbol{\zeta}_2$ in (5.3), and a simulation with 10^5 paths.

We observe that, despite the higher trigger points, the bond priced under the updated model of (4.1) should be issued at a much lower price than under model (4.2).

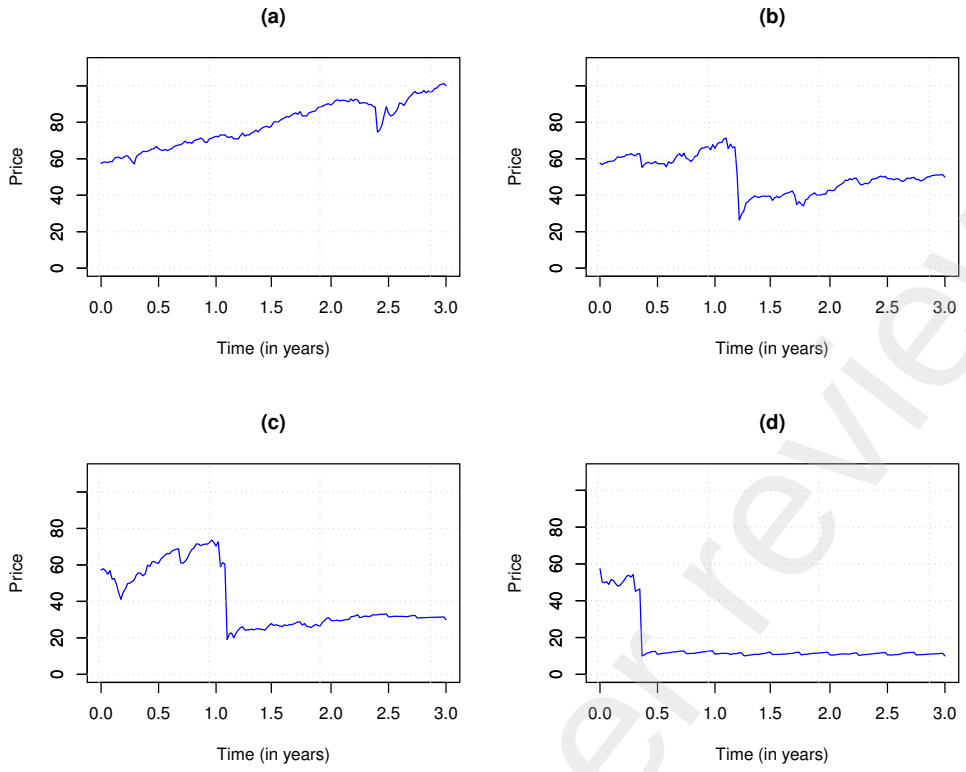

Figure 5.7. This figure shows the price evolutions for a three-year bond with coupons payable quarterly at 6% per annum and attachment and exhaustion points at 0.3 and 0.31, respectively. Each of the graphs (a)–(d) is obtained under a scenario generated for the risk process $\{(r_t, \mu_t)^\intercal\}_{0\le t\le 3}$. The prices are calculated based on formula (5.4), model (4.1), MPR vector $\boldsymbol{\zeta}_1$ in (5.2), and a simulation with 10^5 paths.

Moreover, it is interesting to see that the pandemic experience introduces extra volatility to the post-pandemic mortality risk market, with bond prices that are much more volatile. A comparison of Figures 5.6 and 5.7 shows that while a small change in mortality barely moves the bond price pre-pandemic, it may cause a large swing of the bond price if it occurs post-pandemic. This is not surprising, since in the aftermath of a crisis, even the slightest change in market condition could ripple through the market and stir up turbulences. Mathematically, any mortality change could get amplified through the model—more so under model (4.1) than under model (4.2)—and cause large fluctuations in bond price. For the same reason, the prices obtained under model (4.1) usually recover faster (than under model (4.2)) when the mortality rate surges, triggers the bond, and then returns to its normal range due to mean reversion.

To summarize, one may expect a very different post-pandemic mortality risk market than pre-pandemic. The post-pandemic market will likely see MLS prices that are distressed and more volatile. The distressed price at issuance means a much higher reinsurance premium paid by the MLS sponsor to the bond investors than in the pre-pandemic world. This could change both the supply and demand sides of the MLS market.

5.3 Sensitivity analyses

In this subsection, we conduct sensitivity tests to investigate how the bond issue price would change with respect to some key risk parameters. The bond under consideration is the hypothetical bond defined in Example 3.3, with attachment and exhaustion points set to 0.49 and 0.52, respectively. In our base model, we use (4.1) as the underlying risk process and use $\boldsymbol{\zeta}_1$ as the MPR vector. This ensures that the conclusions hold in the post-pandemic world.

We demonstrate the results in Figures 5.8–5.10. Specifically, Figures 5.8–5.9 show the change of the bond's issue price for varying values of γ_1, γ_2, κ_1, and κ_2, and Figure 5.10 shows the change of the bond price and jump risk elasticity against the change of χ. Here the jump risk elasticity is defined by

$$\frac{dP_0/P_0}{d\chi/\chi}$$

and is calculated using forward difference approximation.

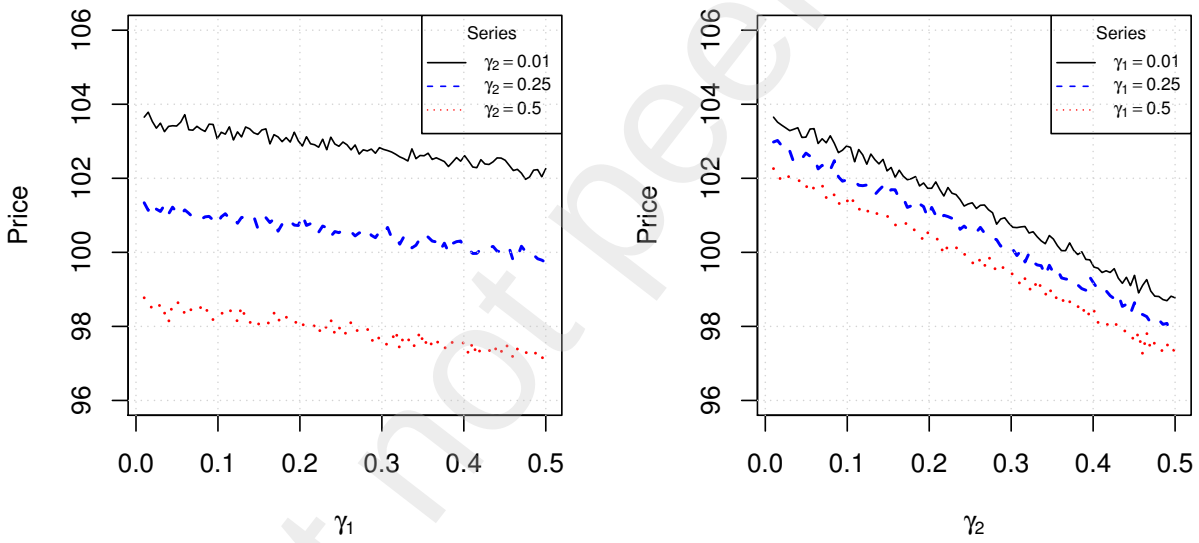

Figure 5.8. This figure shows the change of the hypothetical bond price against varying values of γ_1 and γ_2. In our base model, the process $\{(r_t, \mu_t)^\intercal\}_{0\le t\le T}$ is given by (4.1) and the MPR vector is chosen as $\boldsymbol{\zeta}_1$ in (5.2). The prices are estimated with 10^5 paths of the risk process.

Not surprisingly, we observe that, ceteris paribus, the bond price decreases in any of the MPR parameters. The bond price is more sensitive to changes in the jump risk premium than to the diffusion risk premium. In particular, the impact of jump intensity is quite prominent; a moderate increase in the jump intensity risk premium χ can cause a drastic drop in the bond price. Moreover, the elasticity also decreases, indicating that in the case of a higher jump intensity, the already highly distressed bond price even reacts more strongly to the same change of jump intensity.

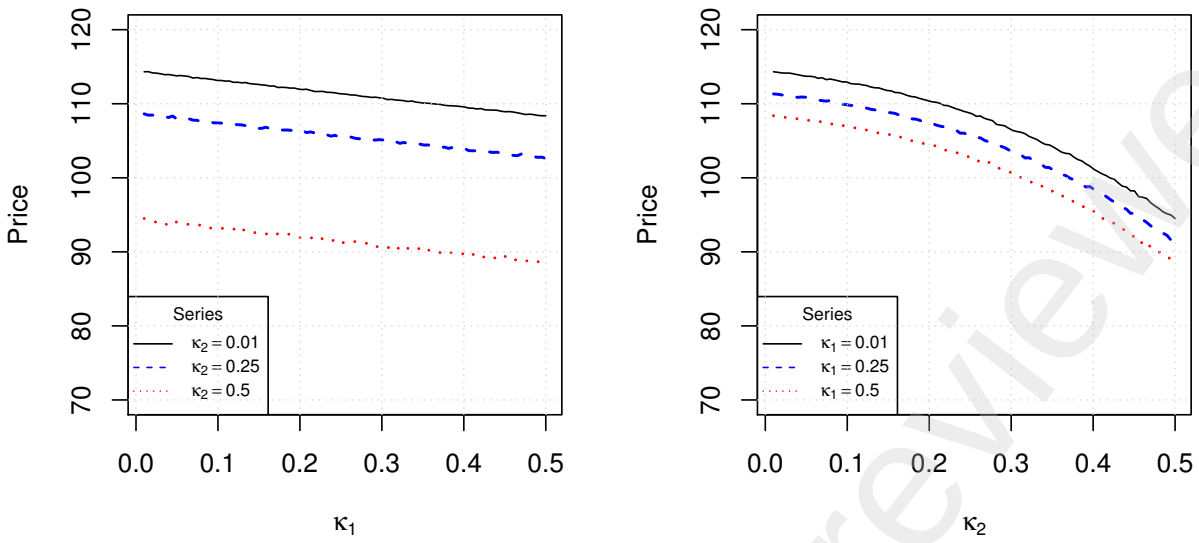

Figure 5.9. This figure shows the change of the hypothetical bond price against varying values of κ_1 and κ_2. In our base model, the process $\{(r_t, \mu_t)^\intercal\}_{0\le t\le T}$ is given by (4.1) and the MPR vector is chosen as $\boldsymbol{\zeta}_1$ in (5.2). The prices are estimated with 10^5 paths of the risk process.

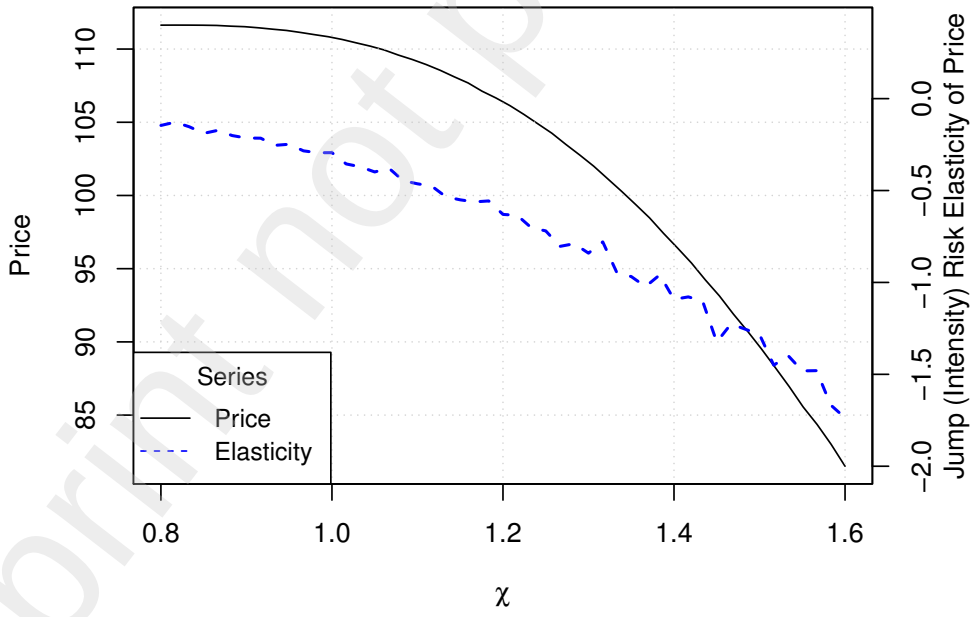

Figure 5.10. This figure shows the changes of the hypothetical bond price and of the jump risk elasticity against varying values of χ. In our base model, the process $\{(r_t, \mu_t)^\intercal\}_{0\le t\le T}$ is given by (4.1) and the MPR vector is set to $\boldsymbol{\zeta}_1$ in (5.2), except that χ varies from 0.8 to 1.6. The prices are estimated with 10^6 paths of the risk process.

6 Concluding remarks

We propose a bivariate AJD structure to jointly model the interest rate and excess mortality and calibrate the model using the most up-to-date US mortality and interest rate data. Our empirical results show that the COVID-19 pandemic experience greatly intensifies the negative instantaneous correlation between the interest rate and excess mortality, which calls for a reassessment of the independence assumption widely used in the literature. Furthermore, we develop a risk-neutral pricing measure that accounts for both a diffusion risk premium and a jump risk premium, and solve for the market prices of risk with second-market indicative mortality bond prices. We argue that failing to recognize the pandemic risk could cost investors dearly, in the sense that they may receive negative mortality risk premia. In addition, based on some envisioned scenarios we show that the pandemic experience is likely to disconcert the MLS prices and reshape the mortality risk market.

During our research, weekly mortality data is available only for four years, which limits us from more in-depth analysis. Consequently, some simplifying assumptions are necessary for model calibration, such as the MPRs and the jump intensity being constant. Another limitation is that some of our conclusions about the post-pandemic market are conjectures that cannot be tested at this stage. Nonetheless, assuming that the mortality risk market continues to grow and timely mortality data of high frequency becomes more accessible, we expect to improve the model and test the conjectures in future research. Lastly, we introduce a three-week lag in the interest rate data to synchronize the first emergency rate cut by the Federal Reserve and the first observed surge in excess mortality at the beginning of the COVID-19 outbreak in the US. Although in the current research such a synchronization can be done by visually inspecting the data, this motivates us to think to incorporate a lag feature into a bivariate model and then establish a statistical procedure to identify the lag. This leads to a novel problem that is both theoretically challenging and practically interesting. We will investigate this problem in a future project, aiming at a rigorous algorithm for detecting joint jumps.

Appendix

A.1 Proof of Proposition 2.1

From Remark 9.3 of Cont and Tankov (2004), we have

$$\begin{aligned}\frac{dZ_{1,t}}{Z_{1,t}} =& \boldsymbol{\Gamma}_t^{\intercal} d\mathbf{W}_t, \\ \frac{dZ_{2,t}}{Z_{2,t-}} =& \sum_{i=1}^{m} d\left(-(\lambda_i^* - \lambda_i)t + \sum_{k=1}^{N_{i,t}} \left(\frac{\lambda_i^*}{\lambda_i} g_i\left(\mathbf{X}_{i,k}\right) - 1\right)\right).\end{aligned}$$

It follows that

$$\frac{d\left(Z_{1,t}Z_{2,t}\right)}{Z_{1,t-}Z_{2,t-}} = \boldsymbol{\Gamma}_t^{\intercal} d\mathbf{W}_t + \sum_{i=1}^{m} d\left(-(\lambda_i^* - \lambda_i)t + \sum_{k=1}^{N_{i,t}} \left(\frac{\lambda_i^*}{\lambda_i} g_i\left(\mathbf{X}_{i,k}\right) - 1\right)\right), \tag{A.1}$$

which indicates that $Z_{1,t}Z_{2,t}$, $0 \le t \le T$, is a martingale under P. Furthermore, we show that $Z_{1,t}Z_{2,t}W_{i,t}^Q$, $0 \le t \le T$, is a martingale under P. For this purpose, we expand

$$d\left(Z_{1,t}Z_{2,t}W_{i,t}^Q\right) = W_{i,t}^Q d\left(Z_{1,t}Z_{2,t}\right) + Z_{1,t}Z_{2,t}dW_{i,t}^Q + d\left(Z_{1,t}Z_{2,t}\right)dW_{i,t}^Q.$$

Then plugging in (2.4) for $d\mathbf{W}_t^Q$ and (A.1) for $d\left(Z_{1,t}Z_{2,t}\right)$, after some simplification we obtain

$$d\left(Z_{1,t}Z_{2,t}W_{i,t}^Q\right) = W_{i,t}^Q d\left(Z_{1,t}Z_{2,t}\right) + Z_{1,t}Z_{2,t}dW_{i,t}.$$

Thus, $Z_{1,t}Z_{2,t}W_{i,t}^Q$, $0 \le t \le T$, is a martingale under P as claimed.

Now we are ready to verify that $\{\mathbf{W}_t^Q\}_{0\le t\le T}$ is a standard bivariate Brownian motion under Q. For any $0 \le s \le t \le T$,

$$E^Q\left[W_{i,t}^Q \middle| \mathcal{F}_s\right] = \frac{1}{Z_{1,s}Z_{2,s}} E\left[W_{i,t}^Q Z_{1,t}Z_{2,t} \middle| \mathcal{F}_s\right] = \frac{1}{Z_{1,s}Z_{2,s}} W_{i,s}^Q Z_{1,s}Z_{2,s} = W_{i,s}^Q,$$

where the first step applies Lemma 5.2.2 of Shreve (2004) and the second step is due to the martingale property of $Z_{1,t}Z_{2,t}W_{i,t}^Q$, $0 \le t \le T$, under P. Thus, $\{W_{i,t}^Q\}_{0\le t\le T}$ is a martingale under Q. Moreover, it has continuous paths, the starting point $W_{i,0}^Q = 0$, and the quadratic variation/covariation

$$\left[W_i^Q, W_j^Q\right](t) = \begin{cases} t, & \text{if } i = j, \\ 0, & \text{if } i \ne j. \end{cases}$$

By Lévy's theorem, $\{\mathbf{W}_t^Q\}_{0\le t\le T}$ is a standard bivariate Brownian motion under Q, as claimed.

Denote by $\mathcal{H}_{i,t}$ the sigma field generated by $\{\mathbf{J}_{i,s}\}_{0\le s\le t}$ for each $i = 1, \ldots, m$ and $0 \le t \le T$, and let

$$Z_{2,i,t} = e^{-(\lambda_i^* - \lambda_i)t} \prod_{k=1}^{N_{i,t}} \left(\frac{\lambda_i^*}{\lambda_i} g_i\left(\mathbf{X}_{i,k}\right)\right), \qquad 0 \le t \le T.$$

For any $\mathcal{H}_{i,T}$ measurable random variable V_i and any bounded measurable function h_i, $i = 1, \ldots, m$, we have

$$\begin{aligned} E^Q\left[\prod_{i=1}^m h_i(V_i)\right] =& E\left[Z_{1,T}Z_{2,T}\prod_{i=1}^m h_i(V_i)\right] \\ =& E\left[Z_{2,T}\prod_{i=1}^m h_i(V_i)E\left[Z_{1,T}\middle|\,\mathcal{H}_{1,T}\vee\cdots\vee\mathcal{H}_{m,T}\right]\right] \\ =& E\left[Z_{2,T}\prod_{i=1}^m h_i(V_i)\right] \\ =& \prod_{i=1}^m E\left[Z_{2,i,T}h_i(V_i)\right]. \end{aligned}$$

This shows that the random variables V_i, $i = 1, \ldots, m$, are mutually independent under Q, and so are $\{\mathbf{J}_{i,t}\}_{0\le t\le T}$, $i = 1, \ldots, m$ under Q. Moreover, for each $i = 1, \ldots, m$, any $\mathcal{H}_{i,T}$ measurable random variable follows a probability law under Q that is distorted by the simplified Radon–Nikodym derivative $Z_{2,i,T}$. Following the proof of Proposition 9.6 of Cont and Tankov (2004), we can show that, under Q, each $\{\mathbf{J}_{i,t}\}_{0\le t\le T}$ is a compound Poisson process with intensity λ_i^* and common jump-size distribution G_i^* for $i = 1, \ldots, m$.

The rest of the proof follows directly by Corollary 11.5.3 of Shreve (2004).

A.2 The price of a risk-free zero-coupon bond

Recall the dynamics of the interest rate process given in (2.10) under Q and the distorted distribution function G^* in Example 2.1. The risk-free zero-coupon bond price is given by

$$P(t,T) = E^Q\left[\exp\left(-\int_t^T r_s ds\right)\middle|\,\mathcal{F}_t^1\right] = e^{\alpha(t)+\beta(t)r_t},$$

where α and β satisfy the ODEs

$$\begin{aligned} 0 &= \alpha'(t) + m_1^*\beta(t) + \frac{1}{2}\sigma_1^2\beta^2(t) + \lambda^*\left(\int_{\mathbb{R}} e^{\beta(t)z}\frac{1}{\sqrt{2\pi}\phi_1}e^{-\frac{(z-\nu_1^*)^2}{2\phi_1^2}}dz - 1\right), \\ 0 &= -1 + \beta'(t) - d_1\beta(t), \end{aligned}$$

with boundary conditions $\alpha(T) = 0$ and $\beta(T) = 0$. Then

$$\begin{aligned} \alpha(t) &= -\frac{m_1^*}{d_1}\left(T - t - \frac{1 - e^{-d_1(T-t)}}{d_1}\right) + \frac{\sigma_1^2}{2d_1^2}\left(T - t - \frac{2\left(1 - e^{-d_1(T-t)}\right)}{d_1} + \frac{1 - e^{-2d_1(T-t)}}{2d_1}\right) \\ &\quad + \lambda^*\int_t^T\left(e^{\nu_1^*\beta(s) + \frac{1}{2}\phi_1^2\beta^2(s)} - 1\right)ds, \\ \beta(t) &= -\frac{1 - e^{-d_1(T-t)}}{d_1}. \end{aligned}$$

The last integral term in $\alpha(t)$ can further be explicitized as

$$\begin{aligned}
&\int_t^T \left(e^{\nu_1^*\beta(s)+\frac{1}{2}\phi_1^2\beta^2(s)}-1\right)ds \\
=\ &\int_t^T \exp\left\{-\nu_1^*\frac{1-e^{-d_1(T-s)}}{d_1}+\frac{1}{2}\frac{\phi_1^2\left(1-e^{-d_1(T-s)}\right)^2}{d_1^2}\right\}ds-(T-t) \\
=\ &\int_0^{T-t} \exp\left\{-\nu_1^*\frac{1-e^{-d_1 w}}{d_1}+\frac{1}{2}\frac{\phi_1^2\left(1-e^{-d_1 w}\right)^2}{d_1^2}\right\}dw-(T-t)\,.
\end{aligned}$$

A.3 Preliminaries for univariate (integrated) Ornstein–Uhlenbeck processes with jumps

In view of the pricing formula (3.2), our numerical procedure requires sampling of the excess mortality, the interest rate, and its integration. To prepare for our sampling algorithm, to be detailed in Subsection A.4, we first provide some preliminary results for univariate (integrated) Ornstein–Uhlenbeck (OU) processes with jumps.

Consider a general OU process $\{x_t\}_{0\le t\le T}$ with jumps that evolves according to

$$dx_t = a\,(b-x_t)\,dt+\sigma dW_t+d\sum_{i=1}^{N_t}\xi_i,$$

where $a\neq 0$, $b\in\mathbb{R}$, and $\sigma>0$ are constants, $\{W_t\}_{0\le t\le T}$ is a standard Brownian motion, $\{N_t\}_{0\le t\le T}$ is a homogeneous Poisson process, and $\{\xi_i\}_{j\in\mathbb{N}}$ is a sequence of i.i.d. normal random variables independent of $\{N_t\}_{0\le t\le T}$. Its solution is given by

$$x_t = x_0e^{-at}+b\left(1-e^{-at}\right)+\sigma e^{-at}\int_0^t e^{as}dW_s+e^{-at}\sum_{i=1}^{N_t}\xi_i e^{a\tau_i},$$

where τ_i is the occurrence time of the ith jump. To derive the exact sampling algorithm for the underlying risk processes, we need the conditional distributions of x_t and $\int_0^t x_s ds$ given the filtration generated by $\{N_s\}_{0\le s\le t}$, $0\le t\le T$.

Obviously, at time t, conditional on $\{N_s\}_{0\le s\le t}$, the random variable x_t as the sum of two independent normal random variables is normally distributed. For $\int_0^t x_s ds$, note that it can be written as

$$\begin{aligned}
&\sigma\int_{s=0}^t\int_{u=0}^s e^{-as}e^{au}dW_u ds+\int_0^t e^{-as}\sum_{i=1}^{N_s}\xi_i e^{a\tau_i}ds+\int_0^t\left(x_0e^{-as}+b\left(1-e^{-as}\right)\right)ds \\
&=I_1+I_2+I_3.
\end{aligned}$$

The term I_3 is deterministic. For I_1, note that

$$I_1 \;=\; \sigma\int_{u=0}^t e^{au}\int_{s=u}^t e^{-as}ds dW_u$$

$$
\begin{aligned}
&= \sigma \int_{u=0}^{t} e^{au} \frac{(e^{-au} - e^{-at})}{a} dW_u \\
&= \frac{\sigma}{a} \int_{u=0}^{t} \left(1 - e^{-a(t-u)}\right) dW_u \\
&= \frac{1}{a} \left(\sigma W_t - \sigma e^{-at} \int_0^t e^{as} dW_s \right), \qquad \text{(A.2)}
\end{aligned}
$$

where in the first step we applied Theorem 64 of Protter (2005). For I_2, let J_ξ be the jump measure of the compound Poisson process $\left\{\sum_{i=1}^{N_t} \xi_i\right\}_{0 \le t \le T}$. We have

$$
\begin{aligned}
I_2 &= \int_{s=0}^{t} e^{-as} \int_{(u,x)\in(0,s]\times\mathbb{R}} x e^{au} J_\xi(du, dx) ds \\
&= \int_{(u,x)\in[0,t]\times\mathbb{R}} x e^{au} \int_{s=u}^{t} e^{-as} ds J_\xi(du, dx) \\
&= \frac{1}{a} \int_{(u,x)\in[0,t]\times\mathbb{R}} x e^{au} \left(e^{-au} - e^{-at}\right) J_\xi(du, dx) \\
&= \frac{1}{a} \int_{(u,x)\in[0,t]\times\mathbb{R}} x - x e^{-a(t-u)} J_\xi(du, dx) \\
&= \frac{1}{a} \left(\sum_{i=1}^{N_t} \xi_i - e^{-at} \sum_{i=1}^{N_t} \xi_i e^{a\tau_i} \right), \qquad \text{(A.3)}
\end{aligned}
$$

where the second step is due to Fubini's theorem. Thus, given the number of jumps by time t and the times of the jump occurrences, the terms I_1 and I_2 are independent and normally distributed. This enables us to derive the exact sampling algorithm below.

A.4 Details of the sampling algorithm

To numerically evaluate the pricing formula (3.2), we need to sample $\{(r_t, \mu_t, R_t)\}_{0 \le t \le T}$ under the Q measure, where $R_t = \int_0^t r_s ds$. Recall the dynamics (2.10) and the distorted distribution function G^* in Example 2.1:

$$
\begin{aligned}
dr_t &= (m_1^* - d_1 r_t) dt + \sigma_1 dW_{1,t}^Q + d \sum_{i=1}^{N_t} X_{1,i}, \\
d\mu_t &= (m_2^* - d_2 \mu_t) dt + \sigma_2 \left(\rho_1 dW_{1,t}^Q + \sqrt{1 - \rho_1^2} dW_{2,t}^Q \right) + d \sum_{i=1}^{N_t} X_{2,i}.
\end{aligned}
$$

The two SDEs and equations (A.2) and (A.3) lead to

$$
r_t = r_0 e^{-d_1 t} + \frac{m_1^*}{d_1} \left(1 - e^{-d_1 t}\right) + \sigma_1 \int_0^t e^{-d_1(t-s)} d\tilde{W}_{1,s}^Q + \sum_{i=1}^{N_t} X_{1,i} e^{-d_1(t-\tau_i)}, \qquad \text{(A.4)}
$$

$$
\mu_t = \mu_0 e^{-d_2 t} + \frac{m_2^*}{d_2} \left(1 - e^{-d_2 t}\right) + \sigma_2 \int_0^t e^{-d_2(t-s)} d\tilde{W}_{2,s}^Q + \sum_{i=1}^{N_t} X_{2,i} e^{-d_2(t-\tau_i)}, \qquad \text{(A.5)}
$$

$$R_t = \int_0^t \left(r_0 e^{-d_1 s} + \frac{m_1^*}{d_1}\left(1 - e^{-d_1 s}\right)\right) ds + \frac{\sigma_1}{d_1}\left(\tilde{W}_{1,t}^Q - \int_0^t e^{-d_1(t-s)} d\tilde{W}_{1,s}^Q\right) + \frac{1}{d_1}\left(\sum_{i=1}^{N_t} X_{1,i} - \sum_{i=1}^{N_t} X_{1,i} e^{-d_1(t-\tau_i)}\right), \tag{A.6}$$

where

$$\tilde{W}_{1,t}^Q = W_{1,t}^Q \qquad \text{and} \qquad \tilde{W}_{2,t}^Q = \rho_1 W_{1,t}^Q + \sqrt{1-\rho_1^2} W_{2,t}^Q.$$

Note that, under Q, $\{\tilde{W}_{1,t}^Q\}_{0\le t\le T}$ and $\{\tilde{W}_{2,t}^Q\}_{0\le t\le T}$ are two standard Brownian motions satisfying $d\tilde{W}_{1,t}^Q d\tilde{W}_{2,t}^Q = \rho_1 dt$, and $(X_{1,i}, X_{2,i})$, $i \in \mathbb{N}$, are i.i.d. copies of a generic bivariate normal random vector $(X_1, X_2) \sim N(\nu_1^*, \nu_2^*; \phi_1, \phi_2; \rho_2)$.

Suppose that, at time $0 \le t < T$, we need to sample in a vectorized way n paths of the processes at, say, m sampling dates t_1, ..., t_m, where $t = t_0 < t_1 < \cdots < t_m = T$. We obtain the samples in m steps, and in step j, $j = 1, \ldots, m$, we use the evolution of the processes over $(t_{j-1}, t_j]$ to sample their time t_j values based on their time t_{j-1} values. Specifically, in step j, we first sample the number of jumps and their occurrence times over $(t_{j-1}, t_j]$, and then sample from the conditional distribution of $\left(r_{t_j}, \mu_{t_j}, R_{t_j}\right)$ given the value of $\left(r_{t_{j-1}}, \mu_{t_{j-1}}, R_{t_{j-1}}\right)$ and the filtration generated by $\{N_s\}_{t_{j-1}<s\le t_j}$.

Consider the jth step and write $\Delta_j = t_j - t_{j-1}$. To sample the diffusion terms in (A.4)–(A.6) over $(t_{j-1}, t_j]$, note that

$$Var^Q\left[\sigma_i \int_{t_{j-1}}^{t_j} e^{-d_i(t_j - s)} d\tilde{W}_{i,s}^Q\right] = \sigma_i^2 e^{-2d_i t_j} \int_{t_{j-1}}^{t_j} e^{2d_i s} ds = \frac{\sigma_i^2\left(1 - e^{-2d_i\Delta_j}\right)}{2d_i}, \quad i = 1, 2.$$

Moreover, for $i = 1, 2$,

$$\begin{aligned} & Cov^Q\left[\sigma_1\left(\tilde{W}_{1,t_j}^Q - \tilde{W}_{1,t_{j-1}}^Q\right), \sigma_i \int_{t_{j-1}}^{t_j} e^{-d_i(t_j-s)} d\tilde{W}_{i,s}^Q\right] \\ = \; & \sigma_1\sigma_i e^{-d_i t_j} Cov^Q\left[\int_{t_{j-1}}^{t_j} d\tilde{W}_{1,s}^Q, \int_{t_{j-1}}^{t_j} e^{d_i s} d\tilde{W}_{i,s}^Q\right] \\ = \; & \sigma_1\sigma_i e^{-d_i t_j} \int_{t_{j-1}}^{t_j} e^{d_i s} dt \left(1_{(i=1)} + \rho_1 1_{(i=2)}\right) \\ = \; & \frac{\sigma_1\sigma_i\left(1 - e^{-d_i\Delta_j}\right)}{d_i}\left(1_{(i=1)} + \rho_1 1_{(i=2)}\right), \end{aligned}$$

and, similarly,

$$Cov^Q\left[\sigma_1 \int_{t_{j-1}}^{t_j} e^{-d_1(t_j-s)} d\tilde{W}_{1,s}^Q, \sigma_2 \int_{t_{j-1}}^{t_j} e^{-d_2(t_j-s)} d\tilde{W}_{2,s}^Q\right] = \frac{\rho_1\sigma_1\sigma_2\left(1 - e^{-(d_1+d_2)\Delta_j}\right)}{d_1 + d_2}.$$

Let $\{(\mathbf{r}_s, \boldsymbol{\mu}_s, \mathbf{R}_s)\}_{t\le s\le T}$ denote n paths of the process $\{(r_s, \mu_s, R_s)\}_{t\le s\le T}$ and note again that we aim to sample the n paths in a vectorized way. We are now ready to present our sampling algorithm as follows:

1. Set $j = 1$.
2. Sample a vector of n Poisson random variables with mean $\lambda^*\Delta_j$, which we denote by $(K_1, \ldots, K_n)$. Here K_i represents the number of jumps over $(t_{j-1}, t_j]$ that occurred on the ith path. Suppose that $\sum_{i=1}^{n} K_i = n_J$.
3. Sample an n_J dimensional vector of independent uniform random variables taking values in $(0, \Delta_j)$, which we denote by $(U_1, \ldots, U_{n_J})$. The components of $(t_j - U_1, \ldots, t_j - U_{n_J})$ constitute a permutation of the occurrence times of the n_J jumps in step 2.
4. Sample n_J i.i.d. copies of the generic pair (X_1, X_2), which we denote by $(X_{1,1}, X_{2,1}), \ldots, (X_{1,n_J}, X_{2,n_J})$.
5. Compute the values of the following three n-dimensional vectors:

$$\mathbf{J}^r = \left(\sum_{i=1}^{K_1} X_{1,i} e^{-d_1 U_i}, \sum_{i=K_1+1}^{K_1+K_2} X_{1,i} e^{-d_1 U_i}, \ldots, \sum_{i=n_J-K_n+1}^{n_J} X_{1,i} e^{-d_1 U_i} \right),$$
$$\mathbf{J}^R = \left(\sum_{i=1}^{K_1} X_{1,i}, \sum_{i=K_1+1}^{K_1+K_2} X_{1,i}, \ldots, \sum_{i=n_J-K_n+1}^{n_J} X_{1,i} \right),$$
$$\mathbf{J}^\mu = \left(\sum_{i=1}^{K_1} X_{2,i} e^{-d_2 U_i}, \sum_{i=K_1+1}^{K_1+K_2} X_{2,i} e^{-d_2 U_i}, \ldots, \sum_{i=n_J-K_n+1}^{n_J} X_{2,i} e^{-d_2 U_i} \right).$$

6. Draw a sample of size n from a 3-dimensional normal random vector that has a zero mean and a covariance matrix with upper triangular matrix

$$\begin{pmatrix} \frac{\sigma_1^2\left(1-e^{-2d_1\Delta_j}\right)}{2d_1} & \frac{\rho_1\sigma_1\sigma_2\left(1-e^{-(d_1+d_2)\Delta_j}\right)}{d_1+d_2} & \frac{\sigma_1^2\left(1-e^{-d_1\Delta_j}\right)}{d_1} \\ & \frac{\sigma_2^2\left(1-e^{-2d_2\Delta_j}\right)}{2d_2} & \frac{\rho_1\sigma_1\sigma_2\left(1-e^{-d_2\Delta_j}\right)}{d_2} \\ & & \sigma_1^2\Delta_j \end{pmatrix}.$$

   Let $\mathbf{Z}^r$, $\mathbf{Z}^\mu$, and $\mathbf{Z}^R$ be the vectors consisting of the components in, respectively, the first, second, and third dimensions of the samples.
7. Let

$$\mathbf{r}_{t_j} = \mathbf{r}_{t_{j-1}} e^{-d_1\Delta_j} + \frac{m_1^*}{d_1}\left(1 - e^{-d_1\Delta_j}\right)\mathbf{1} + \mathbf{Z}^r + \mathbf{J}^r,$$
$$\boldsymbol{\mu}_{t_j} = \boldsymbol{\mu}_{t_{j-1}} e^{-d_2\Delta_j} + \frac{m_2^*}{d_2}\left(1 - e^{-d_2\Delta_j}\right)\mathbf{1} + \mathbf{Z}^\mu + \mathbf{J}^\mu,$$
$$\mathbf{R}_{t_j} = \mathbf{R}_{t_{j-1}} + \int_{t_{j-1}}^{t_j} \left(r_0 e^{-d_1 s} + \frac{m_1^*}{d_1}\left(1 - e^{-d_1 s}\right) \right) ds\mathbf{1} + \frac{\mathbf{Z}^R - \mathbf{Z}^r}{d_1} + \frac{\mathbf{J}^R - \mathbf{J}^r}{d_1},$$

   where $\mathbf{1}$ denotes an n-dimensional vector with all components being 1.
8. Repeat steps 2–7 of the procedure for the time intervals $(t_j, t_{j+1}]$, …, $(t_{m-1}, T]$.

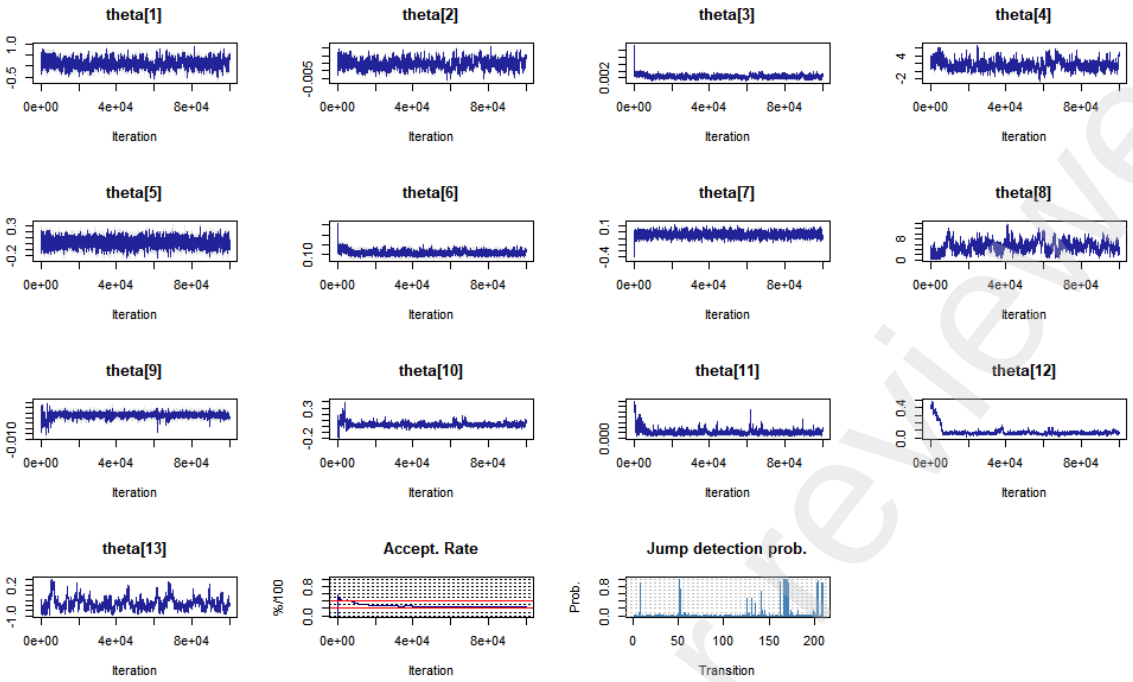

Figure A.1. This figure shows convergence diagnostics for the MCMC sampler. The first 13 panels are trace plots of MCMC draws each corresponding to a single parameter in model (4.1), the final two panels show the evolution of the acceptance rate over the MCMC sampler and jump detection probabilities respectively.

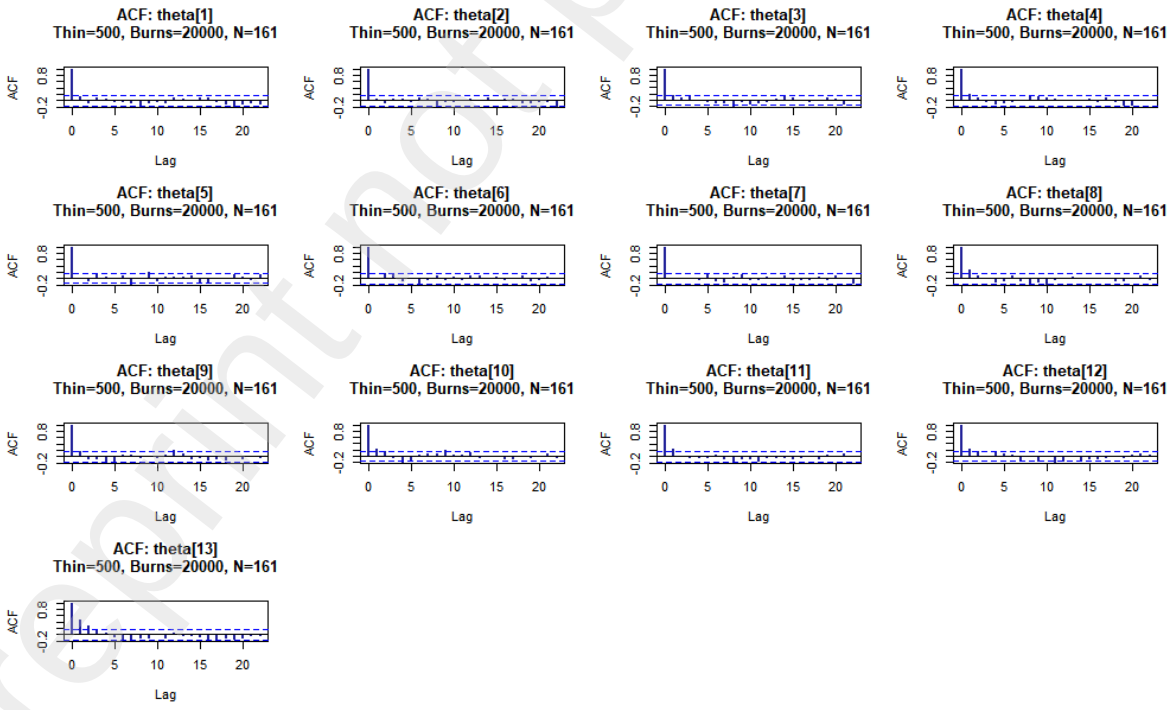

Figure A.2. This figure shows the ACF of MCMC draws for each parameter in model (4.1).

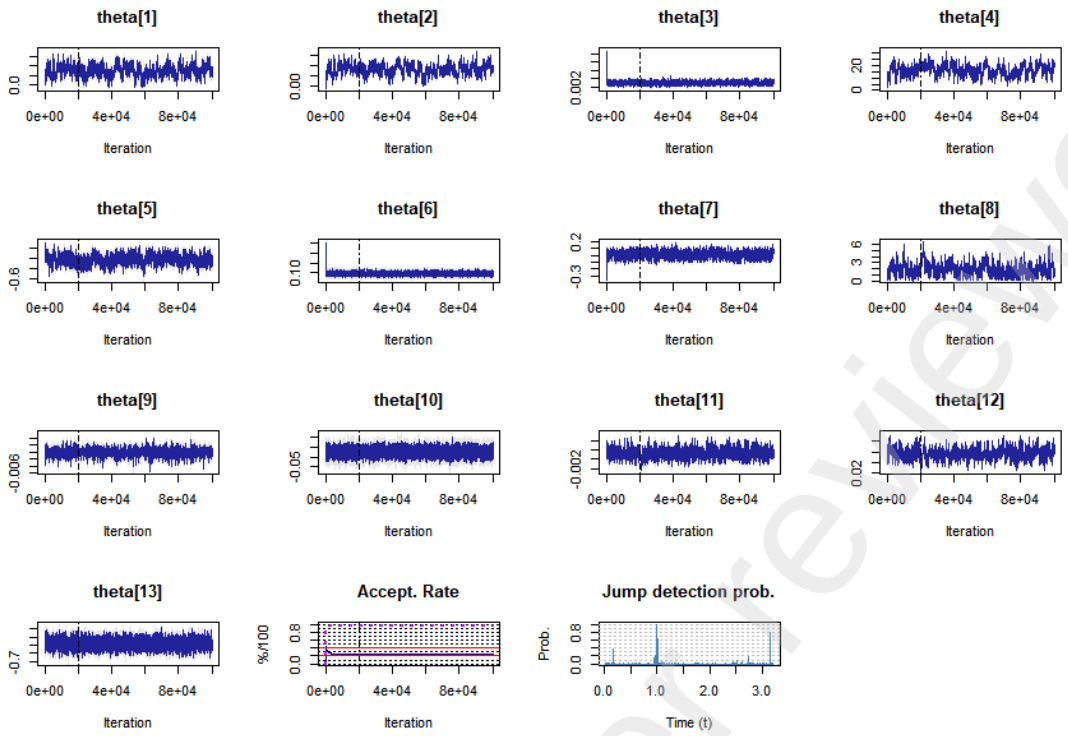

Figure A.3. This figure shows convergence diagnostics for the MCMC sampler. The first 13 panels are trace plots of MCMC draws each corresponding to a single parameter in model (4.2), the final two panels show the evolution of the acceptance rate over the MCMC sampler and jump detection probabilities respectively.

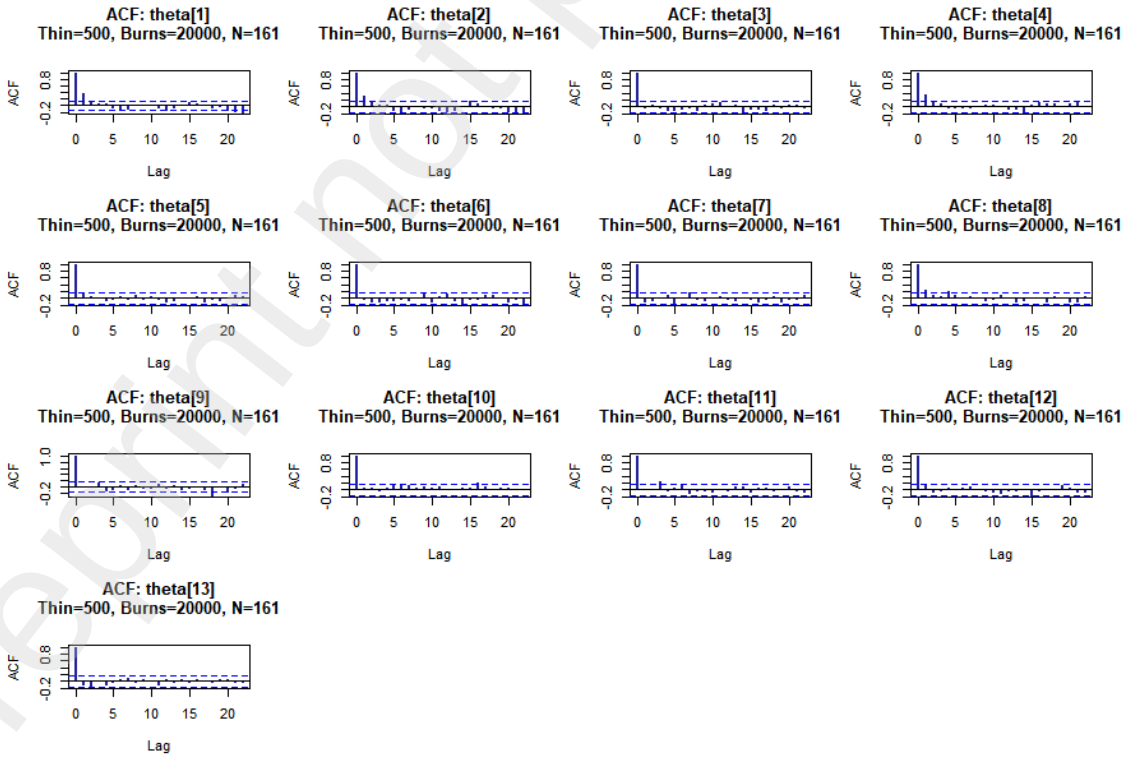

Figure A.4. This figure shows the ACF of MCMC draws for each parameter in model (4.2).

References

[1] Barrieu, P. and Albertini, L., 2009. The Handbook of Insurance-Linked Securities. John Wiley & Sons.

[2] Bates, D.S., 1996. Jumps and stochastic volatility: Exchange rate processes implicit in Deutsche Mark options. The Review of Financial Studies, 9(1), pp.69-107.

[3] Bauer, D. and Kramer, F., 2016. The risk of a mortality catastrophe. Journal of Business & Economic Statistics, 34(3), pp.391-405.

[4] Bayraktar, E., Milevsky, M.A., Promislow, S.D. and Young, V.R., 2009. Valuation of mortality risk via the instantaneous Sharpe ratio: Applications to life annuities. Journal of Economic Dynamics and Control, 33(3), pp.676-691.

[5] Biffis, E., 2005. Affine processes for dynamic mortality and actuarial valuations. Insurance: Mathematics and Economics, 37(3), pp.443-468.

[6] Björk, T., Kabanov, Y. and Runggaldier, W., 1997. Bond market structure in the presence of marked point processes. Mathematical Finance, 7(2), pp.211-239.

[7] Blake, D. and Cairns, A.J., 2021. Longevity risk and capital markets: The 2019-20 update. Insurance: Mathematics and Economics, 99, pp.395-439.

[8] Braun, A., Ammar, S.B. and Eling, M., 2019. Asset pricing and extreme event risk: Common factors in ILS fund returns. Journal of Banking & Finance, 102, pp.59-78.

[9] Chen, A., Hentschel, F. and Klein, J.K., 2015. A utility- and CPT-based comparison of life insurance contracts with guarantees. Journal of Banking & Finance, 61, pp.327-339.

[10] Cont R. and Tankov, P., 2004. Financial Modelling with Jump Processes. Chapman & Hall/CRC Press.

[11] Cox, S. H., Lin, Y. and Wang, S., 2006. Multivariate exponential tilting and pricing implications for mortality securitization. Journal of Risk and Insurance, 73(4), pp.719-736.

[12] Cummins, J.D., 2008. CAT bonds and other risk-linked securities: State of the market and recent developments. Risk Management and Insurance Review, 11(1), pp.23-47.

[13] Dai, Q. and Singleton, K.J., 2000. Specification analysis of affine term structure models. The Journal of Finance, 55(5), pp.1943-1978.

[14] Deng, Y., Brockett, P.L. and MacMinn, R.D., 2012. Longevity/mortality risk modeling and securities pricing. Journal of Risk and Insurance, 79(3), pp.697-721.

[15] Duffee, G.R., 2002. Term premia and interest rate forecasts in affine models. The Journal of Finance, 57(1), pp.405-443.

[16] Duffie, D., 2005. Credit risk modeling with affine processes. Journal of Banking & Finance, 29(11), pp.2751-2802

[17] Duffie, D., Pan, J. and Singleton, K., 2000. Transform analysis and asset pricing for affine jump-diffusions. Econometrica, 68(6), pp.1343-1376.

[18] Eraker, B., 2004. Do stock prices and volatility jump? Reconciling evidence from spot and option prices. The Journal of Finance, 59(3), pp.1367-1403.

[19] Galeotti, M., Gürtler, M. and Winkelvos, C., 2013. Accuracy of premium calculation models for CAT bonds—an empirical analysis. Journal of Risk and Insurance, 80(2), pp.401-421.

[20] Hunt, A. and Blake, D., 2015. Modelling longevity bonds: Analysing the Swiss Re Kortis bond. Insurance: Mathematics and Economics, 63, pp.12-29.

[21] Jacod, J. and Shiryaev A.N., 2003. Limit Theorems for Stochastic Processes (Vol. 288). Springer Science & Business Media.

[22] Jarrow, R.A., Lando, D. and Yu, F., 2005. Default risk and diversification: Theory and empirical implications. Mathematical Finance, 15(1), pp.1-26.

[23] Kallenberg, O., 1997. Foundations of Modern Probability. New York: Springer.

[24] Klebaner, F.C., 2012. Introduction to Stochastic Calculus with Applications. World Scientific Publishing Company.

[25] Kou, S.G., 2002. A jump-diffusion model for option pricing. Management Science, 48(8), pp.1086-1101.

[26] Lando, D., 2009. Credit Risk Modeling: Theory and Applications. Princeton University Press.

[27] Li, H. and Tang, Q., 2019. Analyzing mortality bond indexes via hierarchical forecast reconciliation. ASTIN Bulletin, 49(3), pp.823-846.

[28] Li, H. and Tang, Q., 2021. Joint extremes in temperature and mortality: A bivariate POT approach. North American Actuarial Journal, to appear.

[29] Lin, Y. and Cox, S.H., 2008. Securitization of catastrophe mortality risks. Insurance: Mathematics and Economics, 42(2), pp.628-637.

[30] Lin, Y., Liu, S. and Yu, J., 2013. Pricing mortality securities with correlated mortality indexes. Journal of Risk and Insurance, 80(4), pp.921-948.

[31] Liu, H., Tang, Q. and Yuan, Z., 2021. Indifference pricing of insurance-linked securities in a multi-period model. European Journal of Operational Research, 289(2), pp.793-805.

[32] Menoncin, F. and Regis, L., 2020. Optimal life-cycle labour supply, consumption, and investment: The role of longevity-linked assets. Journal of Banking & Finance, 120, 105935.

[33] Øksendal, B. and Sulem, A., 2005. Applied Stochastic Control of Jump Diffusions. Berlin: Springer.

[34] Pan, J., 2002. The jump-risk premia implicit in options: Evidence from an integrated time-series study. Journal of Financial Economics, 63(1), pp.3-50.

[35] Pienaar, E. and Varughese, M., 2016. Likelihood inference for non-linear, multivariate jump diffusions with state-dependent intensity. Technical Report.

[36] Protter, P.E., 2005. Stochastic Integration and Differential Equations. Springer, Berlin, Heidelberg.

[37] Schönbucher, P.J., 1998. Term structure modelling of defaultable bonds. Review of Derivatives Research, 2(2-3), pp.161-192.

[38] Shreve, S.E., 2004. Stochastic Calculus for Finance II: Continuous-Time Models. Springer Science & Business Media.

[39] Tang, Q. and Yuan, Z., 2019. CAT bond pricing under a product probability measure with POT risk characterization. ASTIN Bulletin, 49(2), pp.457-490.

[40] Wang, S., 2007. Normalized exponential tilting: Pricing and measuring multivariate risks. North American Actuarial Journal, 11(3), pp.89-99.

[41] Xu, Y., Sherris, M. and Ziveyi, J., 2020. Market price of longevity risk for a multi-cohort mortality model with application to longevity bond option pricing. Journal of Risk and Insurance, 87(3), pp.571-595.

Han Li
Department of Actuarial Studies and Business Analytics
Macquarie Business School
Macquarie University
Sydney, NSW 2109, Australia
Email: han.li@mq.edu.au

Haibo Liu
School of Risk and Actuarial Studies
UNSW Business School
UNSW Sydney
Sydney, NSW 2052, Australia
Email: haibo.liu1@unsw.edu.au

Department of Statistics and Department of Mathematics
Purdue University
150 N. University Street
West Lafayette, IN 47907, USA

Qihe Tang
School of Risk and Actuarial Studies
UNSW Business School
UNSW Sydney
Sydney, NSW 2052, Australia
Email: qihe.tang@unsw.edu.au

Zhongyi Yuan (*corresponding author*)
Department of Risk Management
Smeal College of Business
The Pennsylvania State University
University Park, PA 16802, U.S.A.
Email: zhongyi-yuan@psu.edu